Using tectonic block modeling to quantify the impact of potentially–active faults on seismic hazard and risk in western Canada

Richard Styron[1], **Tiegan E Hobbs**[2,3,4], **Murray Journeay**[2]

[1]Global Earthquake Model (GEM) Foundation, [2]Geological Survey of Canada, [3]University of British Columbia, [4]University of Victoria

Non-peer reviewed **Research Article** submitted to SEISMICA

Using tectonic block modeling to quantify the impact of potentially–active faults on seismic hazard and risk in western Canada

Richard Styron * [1], **Tiegan E Hobbs** [2,3,4], **Murray Journeay** [2]

[1]Global Earthquake Model (GEM) Foundation, [2]Geological Survey of Canada, [3]University of British Columbia, [4]University of Victoria

1 Abstract

In order to understand the impact of large, potentially active faults on seismic hazard and risk in western Canada, faults in the region are characterized using a geodetic-geologic block model. The results are then integrated into Canada's existing national seismic hazard and risk models. To do this, potentially active faults are mapped to build a block model around them; then, several thousand geodetic velocities and several hundred Quaternary geologic slip rates are inverted to estimate slip rates on the mapped faults. The block model yields low to moderate slip rates (<2 mm/yr) on most faults, except along the Queen Charlotte and Denali fault systems. These faults are then incorporated into Canada's 6th Generation Seismic Hazard Model and changes in hazard and risk at key population centers are evaluated. While absolute changes in hazard are modest in most locations, relative increases of several times the original hazard levels are found at sites near newly-added faults, especially in the eastern portion of the study region. Risk modeling indicates potential increases in expected losses, with some communities showing >10 times higher losses at the 475–year return period. However, the sparsity of geodetic and geologic data across much of western Canada significantly limits confidence in these results. Our findings suggest that these or similar faults may pose meaningful hazard, and that additional geodetic monitoring and geologic investigation are urgently needed to better constrain their activity and impact on seismic hazard and risk across the region.

2 Introduction

2.1 Motivation

The Canadian Cordillera, which extends from the Pacific coast to the eastern edge of the Rocky Mountains (Cassidy et al., 2010), is enigmatic in that while it is bounded by a rapidly deforming plate boundary, and in places yields clear evidence for deformation up to 1000 km inboard from the plate margin (e.g. the Nahanni earthquake sequence of 1985; Horner et al., 1990), for much of its great extent, unambiguous geological and geophysical documentation of moderate to large magnitude seismicity is lacking. Very few active faults have been positively identified, in part due to the ruggedness and inaccessibility of the terrain, the sparsity of the population, and the apparent slow strain rates across much of the region.

*Corresponding author: richard.styron@globalquakemodel.org

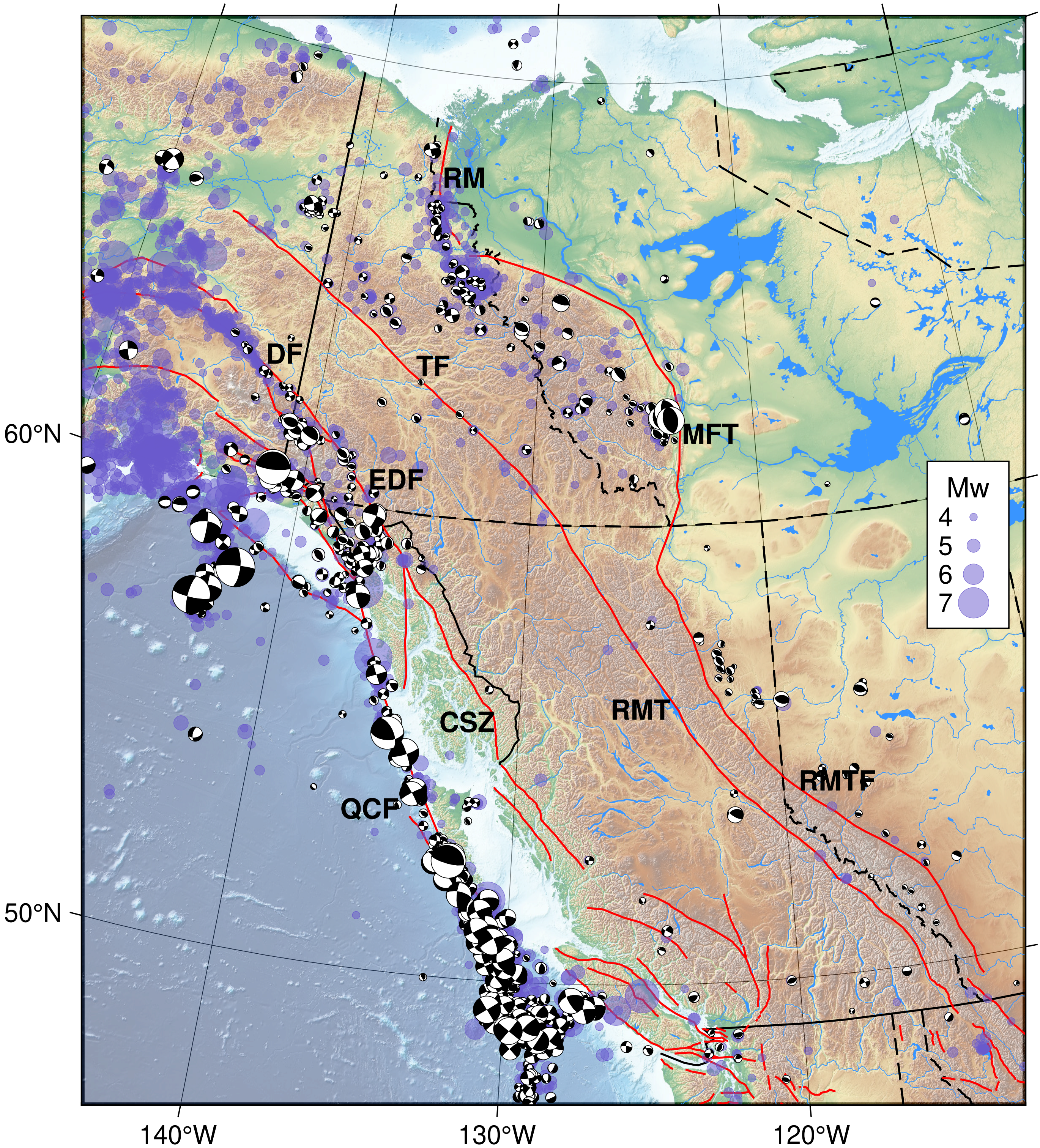

Figure 1 Seismicity and faults in western Canada and vicinity above 30 km depth. Focal mechanisms are from the the updated catalog by Kao et al. (2012) (1995-present) and the GCMT catalog (Ekström et al., 2012). Purple dots are from the SHEEF catalog (prehistory-2010) (Halchuk et al., 2015b). Scale is based on magnitude and is the same. Faults in this study are shown in orange. DF=Denali fault. TF=Tintina fault. EDF=Eastern Denali fault. MFT=Mackenzie frontal thrust. RMT=Rocky Mountain Trench. RMTF=Rocky Mountain thrust front. CSZ=Coast Shear Zone. QCF=Queen Charlotte Fault.

As a consequence of the lack of fault characterization, Canada's Seismic Hazard Model (CanSHM) contains very few crustal fault sources within the North American plate, apart from those that represent the rapidly slipping and relatively well–known Queen Charlotte, Denali, and Tintina faults that cross the Alaskan border. Recent work has helped identify additional active structures closer to cities, such as the Leech River and X̲EOLX̲ELEK–Elk Lake Faults (Morell et al., 2018; Harrichhausen et al., 2021, 2023), the former of which has already been added to the CanSHM. However, best practices in the construction of seismic hazards models promote the use of fault sources in addition to distributed seismicity sources (e.g., Gerstenberger et al., 2020), where applicable.

The development of a seismic hazard model with more defined fault sources, in addition to area sources calibrated to the instrumental seismic catalog, would be especially beneficial in Canada in terms of modeled seismicity beyond what can be known from the catalog, which only extends for approximately 70-150 years in much of the west (Basham and Newitt, 1993; Allen and Brillon, 2015; Bent et al., 2018; Kolaj et al., 2020). The location, geometry, and kinematics of modeled ruptures can be known more accurately on individual faults versus averages throughout a crustal volume, and the slip rates of faults provide a better estimate of the rates of damaging seismicity, especially in slowly–deforming regions where the catalog length is much shorter than the mean recurrence intervals of large earthquakes.

The Canadian Cordillera hosts a number of large, well–located faults that may be considered 'potentially active', meaning that they are not definitively demonstrated to be seismically active nor inactive, as well as a few faults known to be active but still represented primarily as area sources in the existing seismic hazard models due to a lack of information about their recurrence, magnitude, and/or geometry. The recognition of this class of faults motivates us to consider their possible impacts on the seismic hazard and risk of the region, to provide stakeholders with precise and quantitative information on these potential impacts, and to generally understand whether improved characterization of faults in western Canada is likely to significantly affect the seismic hazard and risk throughout the region.

In the absence of high resolution studies characterizing individual faults, modern geodetic and topographic datasets can be leveraged to characterize faulting in a region with sufficient accuracy to construct a regional fault source model for seismic hazard and risk modeling (e.g., Gerstenberger et al., 2020), for demonstration of the latter goal.

2.2 Evidence for upper plate deformation

2.2.1 Seismicity

Seismicity is present throughout western Canada (Figure 1). The vast majority of the seismicity is localized on the North America–Pacific plate boundary faults: the Cascadia subduction zone, the Queen Charlotte Fault (QCF) and the Alaska–Aleutian subduction zone. Moving inland, a belt of seismicity extends north along strike of the Fairweather-QCF system through the complex deformation zone of the Wrangell and St. Elias Mountains, and north to the Denali fault along the Totschunda, Connector, and Duke River Faults (though substantial seismicity is also present on the Eastern Denali fault, southeast of this junction; Doser, 2014).

Farther inland, seismicity exists throughout the northern Cordillera in the Yukon and the Mackenzie Mountains along the Mackenzie Mountain Front in the Northwest Territories (NWT) (Drooff and Freymueller, 2023), particularly in the Nahanni and Richardson Mountains regions (Hyndman et al., 2005). The Nahanni earthquake sequence began in 1985, with magnitudes up to moment magnitude (M_w) 6.7. Focal mechanisms (Ekström et al., 2012) and aftershock distributions (Horner et al., 1990) indicate thrusting on a shallowly west–dipping plane. Seismicity in the Richardson Mountains is more abundant and spread over a larger region, with the largest events (also mid M 6 events) occurring in 1940 (Cassidy and Bent, 1993). In this region, seismicity appears to be localized onto narrow fault bands within the Richardson Anticlinorium and Selwyn Basin (Drooff and Freymueller, 2023).

Moderate-magnitude seismicity is also found throughout the Yukon, especially along the Tintina fault (Drooff and Freymueller, 2023). The density of seismicity drops off noticeably south of the British Columbia (BC) border (Figure 1). Nonetheless, moderate earthquakes have been observed over much of BC and western Alberta (AB) (e.g., Milne, 1970; Rogers and Ellis, 1979; Cassidy et al., 2010; Dokht et al., 2020), both along the major faults and into the Canadian shield. The few focal mechanisms indicate NE-SW contraction, consistent with thrusting on the Rocky Mountain thrust front (Ristau et al., 2007; Finley et al., 2023).

Seismicity is also present near Vancouver Island and the Salish Sea region of southwestern BC and northern Washington State (e.g. Barrie and Greene, 2018; Greene et al., 2018; Harrichhausen et al., 2021, 2023) (Figure 2). The largest known earthquake in the region is the 1946 M_w 7.3 Vancouver Island earthquake (Rogers and Hasegawa, 1978), which may have occurred on the Beaufort Range Fault (Lynch et al., 2025; Lynch, 2023) or in the subducting slab (Rogers and Hasegawa, 1978). Other earthquakes have been recorded near the West Coast Fault (Muller et al., 1981; Finley et al., 2023) and Nootka Fault Zone (Merrill et al., 2022), indicating active deformation in the North American plate above the Cascadia subduction zone interface.

2.2.2 Geodesy

Geodetic velocities in northwestern North America (Figure 3) broadly reflect interseismic strain accumulation in the Cascadia and Alaska–Aleutian subduction zones (including the collision of the Yakutat block with southeastern Alaska) and along the QCF (Mazzotti and Hyndman, 2002; Mazzotti et al., 2003; McCaffrey et al., 2013; Elliott and Freymueller, 2020; Evans, 2022). However, just as with the spatial distribution of seismicity, there is clear geodetic evidence of substantial crustal deformation hundreds of kilometers inboard from the plate interface in parts of western Canada, although the signals are muted, and there are signs of stability in the data elsewhere, with large data gaps in the interior of BC precluding clear delineation of these zones. North of about 58°, Global Navigation Satellite System (GNSS) velocity vectors show clear east-northeast–directed motion that is readily interpretable as east–west crustal shortening in the Mackenzie range (Hyndman et al., 2005; Leonard et al., 2007).

In the southern Canadian Cordillera (Figure 4), a clear northeastern trend in the velocity field continues through the interior from northwestern Washington (WA). This trend is visible into the Alberta Rockies, suggesting slow shortening along the frontal thrusts of the Rockies at this latitude. Though the azimuth of the velocities with respect to stable North America is consistent with the convergence direction of the Juan de Fuca plate, the magnitude of the velocities stay higher for a much farther distance inboard than expected from a locked Cascadia subduction interface. This is shown by modelled GNSS velocities resulting from a fully-locked Cascadia subduction zone, as shown in Figure S1.

Crustal motion also seems to decrease northward, with little apparent motion of few stations in the central interior of BC with respect to stable North America north of 53°N, although there is only one GNSS station (in Smithers, BC)

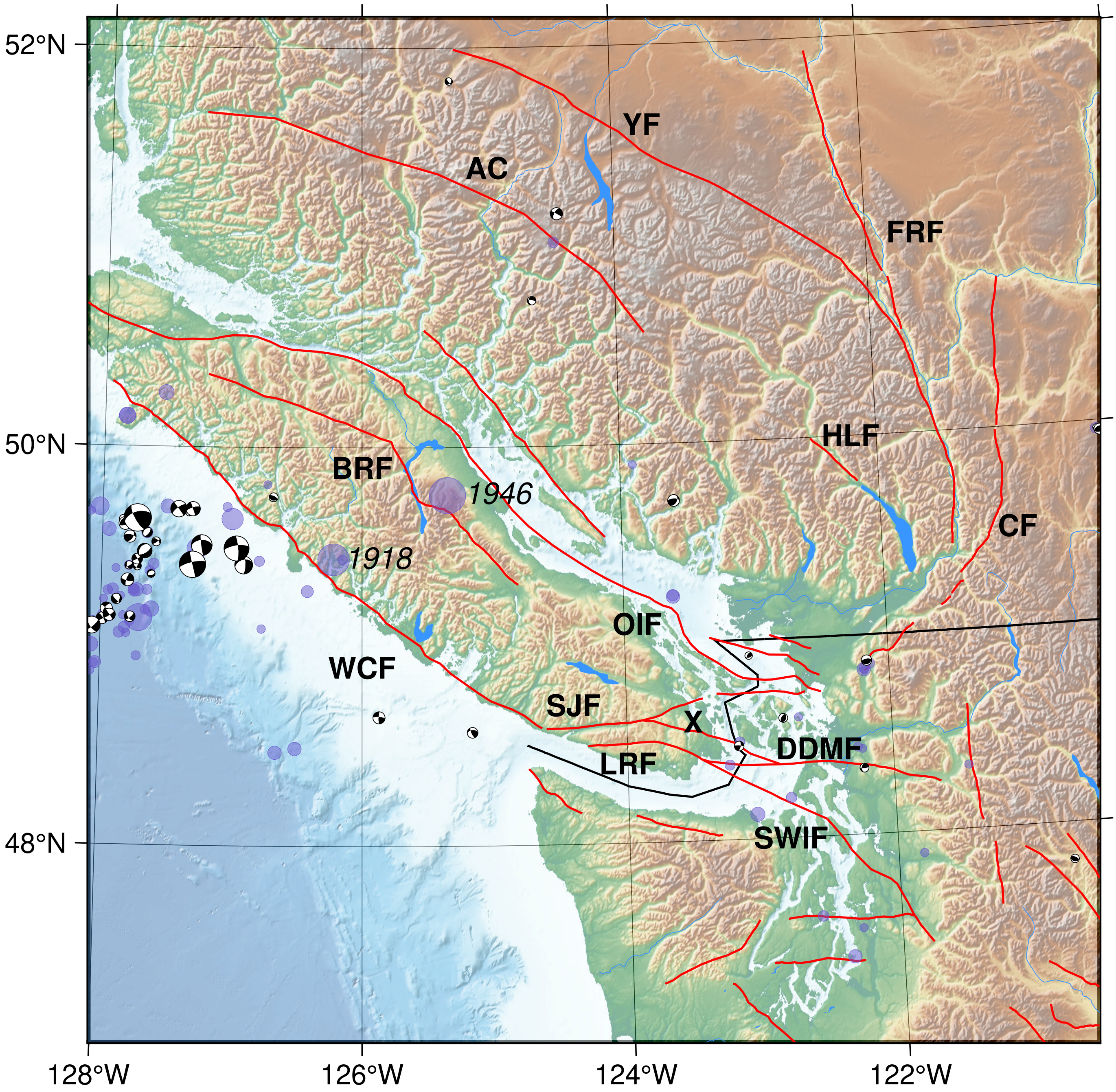

Figure 2 Same data as Figure 1, but focused on southwestern BC and the Puget Sound region. YF=Yalakom fault. AC=Ascent Creek fault. FRF=Fraser River fault. HLF=Harrison Lake fault. CF=Coquihalla fault. BRF=Beaufort Range fault. OIF=Outer Islands fault zone. WCF=West Coast fault. SJF=San Juan fault. X=XEOLXELEK–Elk Lake fault. LRF=Leech River fault. DDMF=Darrington-Devils Mountain fault. SWIF=South Whidbey Islands fault. Dates in italics are the years of earthquakes on Vancouver Island referred to in the text.

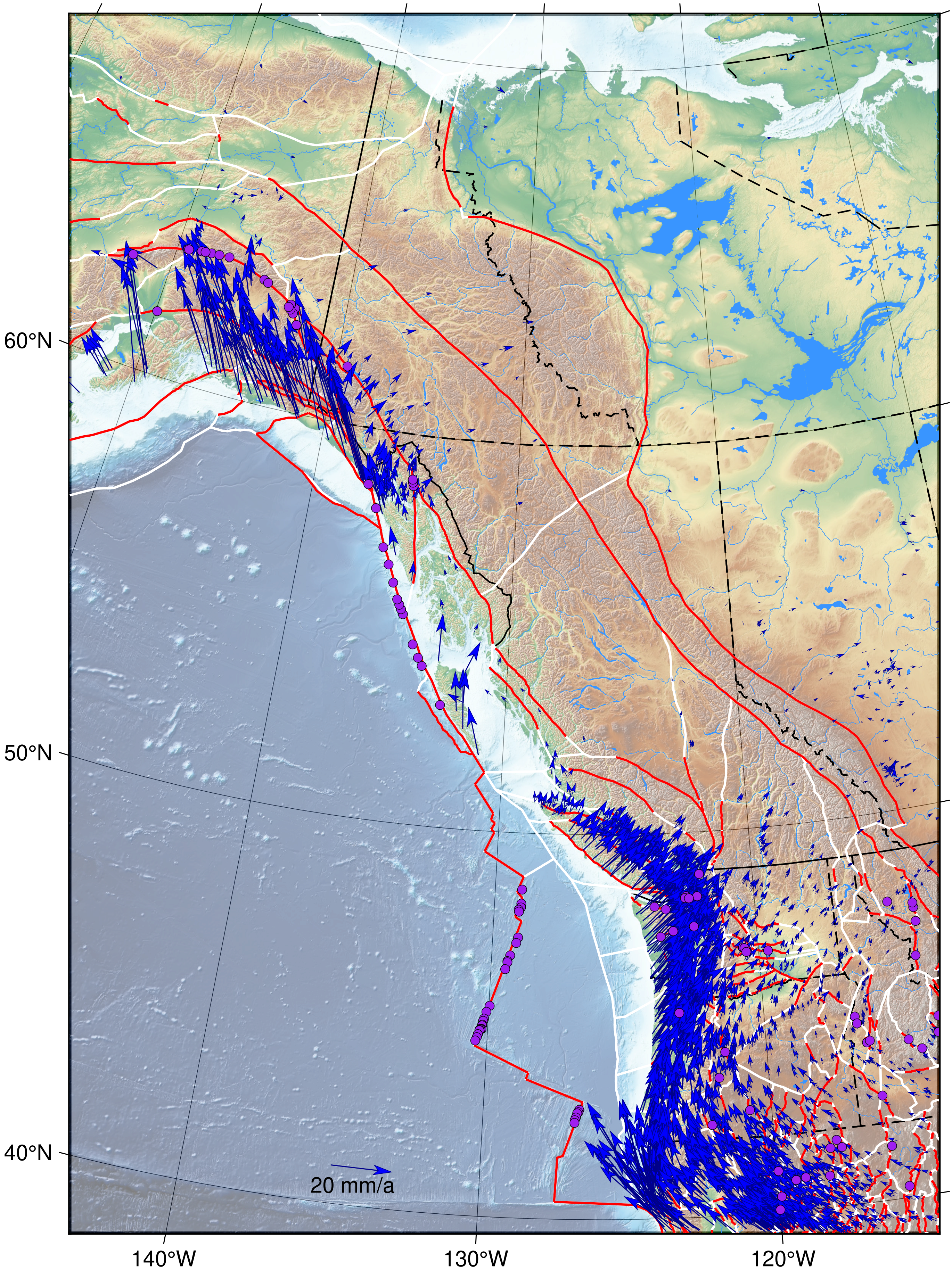

Figure 3 Geodetic data across study region, used in block inversion. Blue vectors represent GNSS velocities. Velocity errors are omitted for clarity. Purple points represent geologic slip rates. See Section 3.2.1 for details of datasets used herein.

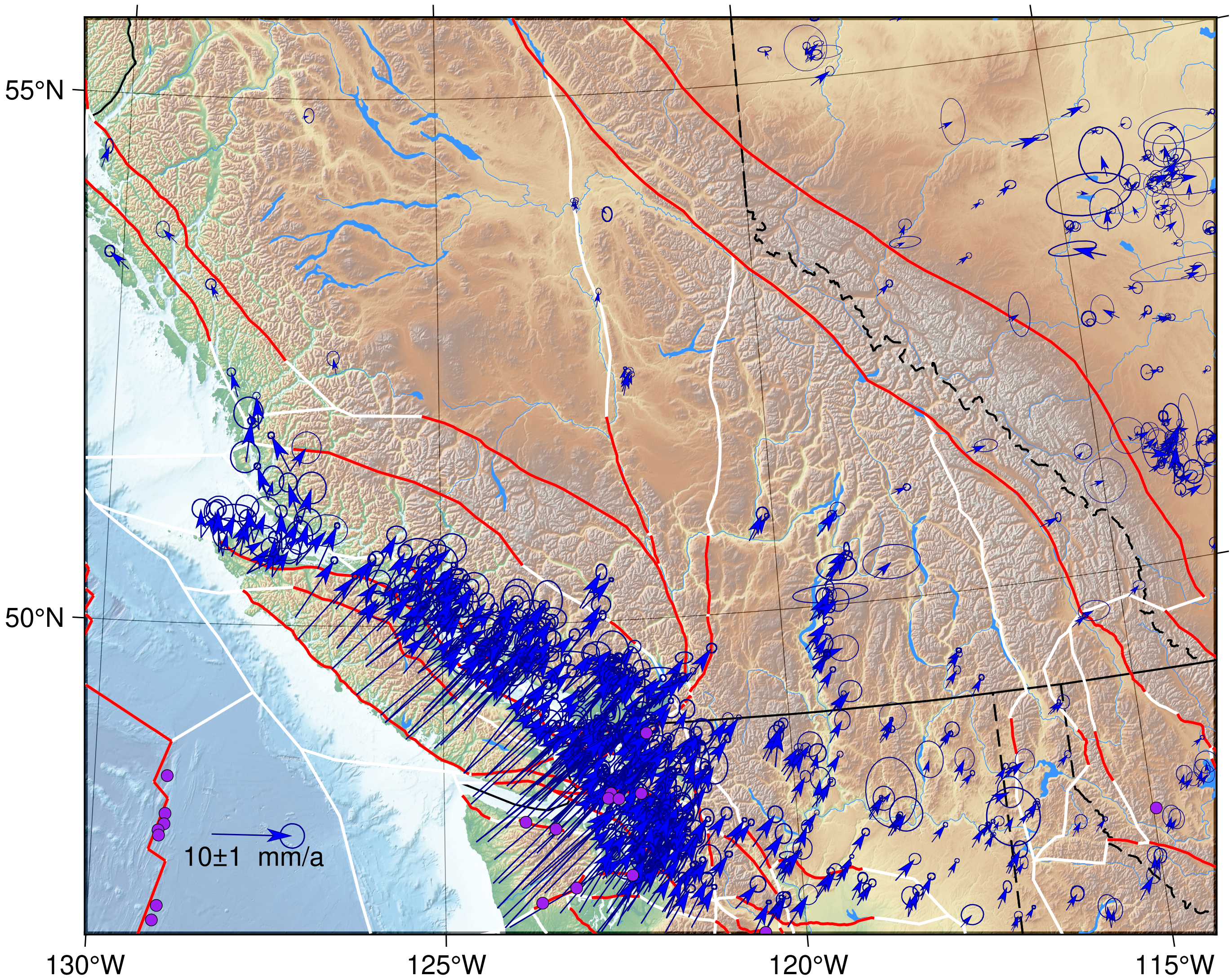

Figure 4 Same as Figure 3 but for southern British Columbia and vicinity. GNSS velocities shown as blue arrows, with 1-σ error ellipses (see Section 3.2.1 for details).

in the 675 km distance between Prince George and Dease Lake, and between Prince Rupert on the coast to the far side of the deformation front in the east. This data gap inhibits assessment of the transfer of strain evident in the southern and northern Canadian Rockies in the central Rockies (e.g. Ristau et al., 2007); strain could be transferred west to the Coast Shear Zone along unknown structures in northern and southern BC, or shortening could continue along the length of the Rocky Mountain thrust front.

To better quantify crustal strain across western Canada and its impact on seismic hazard, a block model is created based on a provisional mapping of potentially active crustal fault structures. The block model is then converted into a probabilistic seismic hazard model, and a risk assessment is completed to demonstrate the potential impacts of geodetic data in understanding the threat of earthquakes across western Canada.

3 Methods and Results

We must first characterize faulting throughout western Canada, then integrate those faults into the existing seismic source model. To perform the former, we map potentially active faults and construct a block (tectonic microplate) model to quantify their kinematics and activity rates. Then, fault sources were constructed from the block model using new methods from the Global Earthquake Model Foundation (GEM). Finally, the new sources were combined with the existing seismic source model by adding the new fault sources and modifying or replacing specific affected sources from the original model, as appropriate.

It must be noted that combining sources in this way is not ideal; more commonly, both fault and distributed seismic sources are built together to maximize congruence and minimize gaps and overlaps in coverage (e.g., Gerstenberger et al., 2020). However, such an approach requires building the entirety of the seismic source model for western Canada and surroundings from scratch, which is both outside the scope of this project, and runs the risk of producing a model sufficiently different than the current model that the specific goal of understanding the role of fault sources is lost. In other words, the goal of this work is to understand how crustal faults and geodetic data might affect CanSHM, not to produce a new hazard model to replace it.

3.1 Fault mapping

The study area has hosted an active plate boundary for hundreds of millions of years (e.g., Monger and Price, 2002), leading to a dense network of bedrock faults throughout the Cordillera. However, little documentation of Quaternary fault activity exists in the Canadian portion of the Cordillera. Herein, faults were mapped (red lines in Figure 3) and associated with known structures in the literature. The fault, block and subduction zone mesh geometries in and around the study area are shown in Figures S2 and S3.

The faults that are the best expressed in the topography are those displaying continuous and youthful (e.g., topographically sharp) tectonic geomorphology. These are mostly the largest faults in the orogen, with the addition of a handful of smaller faults in southwestern BC. Therefore, fault mapping in this study is focused on these larger and more well-defined groups of structures: the frontal faults of the Cordillera (the Mackenzie and Rocky Mountain frontal thrust); the Tintina fault and Rocky Mountain Trench; the Denali fault, Coastal Shear Zone, and connections to the QCF; and the various faults in the complex deformation zone in southwestern BC and adjacent Washington State, from Vancouver Island and the Salish Sea through the Coast Ranges and into the Fraser River region.

Faults were mapped on moderate– to high–resolution topographic data, primarily 30 m SRTM imagery (Van Zyl, 2001) south of 60°N and ArcticDEM (Porter et al., 2018) north of this latitude. Offshore, bathymetry from the GMRT synthesis was used (Drennon et al., 2023). Due to the maturity of many of the fault systems, the traces are often anastomosing, multi–stranded or branching; we have followed the most continuous path in these instances. While it is possible that some structures may be more diffuse fault zones rather than single fault strands, as modeled here, the block modelling approach is less well–suited to high resolution fault strand modelling as it requires data in every block. Therefore, deformation is treated as being localized to single faults, with the caveat that the slip budget could equally be applied across a more diffuse set of parallel structures.

We have chosen a single, continuous trace for the eastern deformation front of the orogen, from the Richardson Mountains south through the Mackenzies and along the Rocky Mountain front. The bedrock geology here displays a highly imbricate stack of thrusts (e.g., Struik, 1988), but there is little reason to assume contemporary out–of–sequence thrusting, given the localization of existing seismicity near the rangefront (Figure 1). Therefore we have represented it as a shallow west–dipping thrust (e.g., Horner et al., 1990; Snyder et al., 2005).

The Tintina fault–Rocky Mountain Trench is continuous throughout Canada, and is mapped as a continuous vertical fault (e.g., Drooff and Freymueller, 2023; Snyder et al., 2005). The Denali fault is mapped from eastern Alaska, through the Yukon and into the Alaskan Panhandle (e.g., Elliott and Freymueller, 2020; Blais-Stevens et al., 2020) where it meets a complex transition zone with the QCF–Fairweather Fault system and Coast Shear Zone via the Totschunda and Connector Faults (Doser, 2014; Gosselin et al., 2024) The Chatham Strait fault branches from the eastern Denali fault/ Coast Shear Zone, connecting to the QCF farther south. Inboard of the Haida Gwaii archipelago, the BC reach of the Coast Shear Zone (Littel and Bostock, 2023) is represented as two parallel strands (selected from many possible strands), about 40 km apart, with a number of GNSS stations measuring the motion within the intermediate crustal block.

Southwestern BC and northwestern WA are the most tectonically complex parts of the study area. The number and spatial density of demonstrably–active and potentially–active faults are much higher here; fortunately, geodetic data are even more numerous and closely–spaced, so that we may resolve block motions and fault slip rates for all of the faults considered.

The westernmost crustal fault is the West Coast Fault (Muller et al., 1981) along the Pacific coast of Vancouver Island. This thrust fault (Balfour et al., 2012; Clowes et al., 1987) is observed in bedrock geology and seismic imagery, and has hot springs along its trace, a common phenomenon for regional-scale faults, especially active faults (Finley et al., 2023). The 1918 M_w6.9 Vancouver Island earthquake was located near the trace (Figure 2), and may be associated with it.

Northeast of the topographic crest of Vancouver Island lies the Beaufort Range fault (Lynch et al., 2025; Lynch, 2023). This structure has a history as an Eocene NE-dipping reverse fault, and is mapped and modeled with this geometry in this study. However, the focal mechanism from the 1946 Vancouver Island earthquake, believed to have occurred on the Beaufort Range fault, suggests right-lateral slip on a steeply dipping plane (Rogers and Hasegawa, 1978). Field investigation by Lynch (2023) similarly indicates right-normal slip on a fault plane that dips steeply near the surface, raising the possibility that the current active fault reactivates the older Eocene fault with a different sense of slip, as was also observed for the Leech-River Fault (Harrichhausen et al., 2021), or reaches the surface in the same location as the older thrust, but may be increasingly separated with depth.

The Outer Islands fault lies between Vancouver Island and the mainland. It is observed in bathymetry and associated with aligned disturbances in near-surface seafloor sediments near Cape Lazo (Barrie et al., 2021; Douglas et al., 2022). It is posited to be associated with microseismicity and a strong NW–trending velocity discontinuity (Ramachandran et al., 2004; Ramachandran, 2012). On its southeastern end, we have mapped it as merging into the Skipjack Island and Lummi faults in the San Juan Islands (Dash et al., 2007). The X̲EOLX̲ELEK–Elk Lake fault, which runs through the Saanich Peninsula and west into Haro Strait (Harrichhausen et al., 2023), is modeled as merging into the Darrington–Devils Mountain fault at its eastern end in this area as well. The Leech River (Morell et al., 2018; Harrichhausen et al., 2021)is also modeled as connecting to the Darrington–Devils Mountain and Southern Whidbey Island faults in WA, as well (Personius et al., 2014; Barrie and Greene, 2018). Both the X̲EOLX̲ELEK–Elk Lake and Leech River Faults have documented Quaternary activity.

Within the Coast Range of BC, a single boundary with discontinuous faults was drawn through the Harrison Lake fault and along to the northwest broadly following the Ascent Creek fault (Journeay and Friedman, 1993). On the northeastern rangefront lies the Yalakom fault (Umhoefer and Schiarizza, 1996), which merges with the Fraser River fault near Lillooet (Coleman and Parrish, 1991). The Fraser River fault continues north and south from this junction; mapping of it stops near the confluence of the Chilcotin river, north of which the fault is less well defined in the topography. East of the southern Fraser River fault, the Coquihalla fault is mapped, continuing north through the Highland Valley copper mine, where the fault has been mapped by Lesage et al. (2019), and up to the Thompson River, north of which it is markedly less distinct.

3.2 Block modeling

Block modeling is a well-established technique for quantifying the rates of deformation in a region, particularly the slip rates of faults bounding around tectonic microplates. The technique is rooted in the very earliest studies of tectonic plate motion on a spherical Earth, from when as few as 8 plates were used (e.g., Chase, 1972). As the mathematics of plate motion on a sphere are unchanged at smaller scales, modern methods include a few updates but are fairly similar: Plates/blocks are contiguous sections of the Earth's crust, bounded by faults, that move with respect to each other. The rates of strain between adjacent blocks are, generally, much higher than the strain rates within the blocks, so that the relative motions of the interiors of the plates may be considered to be accommodated on the faults separating them. Modern updates primarily include the effects of interseismic strain accommodation on geodetic data near the faults (i.e., fault locking effects), the possibility of estimating intra-block strain simultaneously with the block motions, and improvements in the solution strategy through linear algebraic techniques introduced by Meade and Hager (2005) so that the problem may be represented as a linear least squares problem, and the global optimum solution is guaranteed to be found through a typical least-squares direct inversion.

We use methods drawing on this work, as well as (Meade and Loveless, 2009), described in detail by Styron (2022a), using the code *Oiler* (Styron, 2022b). The block model consists of a set of adjacent, rigid blocks. Each block is bound by faults or by off-fault block boundaries, where no fault can be confidently mapped and no elastic locking signal is produced. Faults exist only at block boundaries. The relative motion of adjacent blocks is accommodated entirely on the faults or off-fault block boundaries, such that the slip rates and kinematics of the faults are simply the relative motion of the blocks bounding the faults, resolved on those faults. Additionally, triangular meshes representing subduction zone interfaces are included; unlike the crustal faults between blocks, which are fully locked in the interseismic period, the triangular patches in the subduction zone mesh are allowed to accumulate strain at rates different than the plate rates, such that they may be completely creeping, partially or fully locked (Meade and Loveless, 2009). Spatial regularization of the locking rates is applied to the mesh, so that the rates vary smoothly in space and the problem remains well-posed. The subduction zone mesh for the Alaska–Aleutian subduction zone is based on Hayes et al. (2018), and the mesh for Cascadia is derived from Graham et al. (2018).

Oiler does not use a single reference frame for block motions; instead, all block motions are relative to either a reference frame, which may be a geodetic reference frame, or another block in the model. This allows us to use geodetic data from multiple sources without the need for harmonization, and makes for a simple inclusion of geologic slip rates, which measure the motion of one block relative to another.

Oiler constructs a system of linear equations to simultaneously estimate block motions and subduction zone slip deficits, and solved through a weighted least-squares inversion. The system of equations includes equality constraints

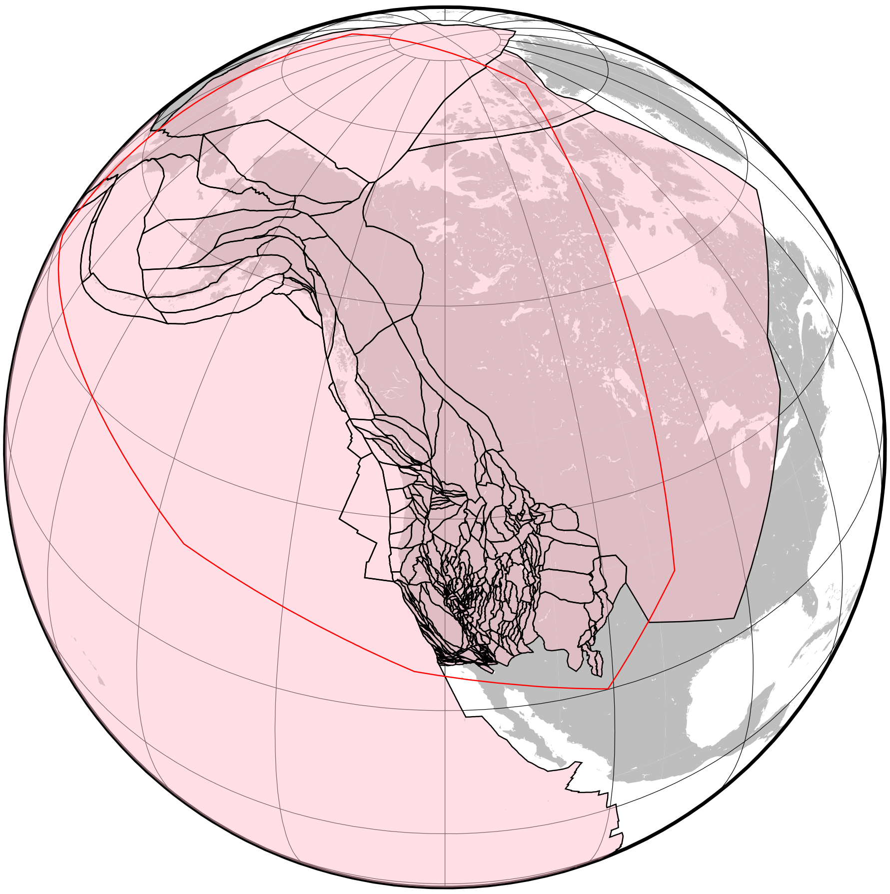

Figure 5 Geometries of all blocks included in the model (pink). The red line shows a polygon that was used to select all blocks from a near–global block and fault compilation.

to ensure complete internal consistency of the block motions, i.e. that all plate motion circuits close (e.g., McKenzie and Parker, 1967; Chase, 1972). The uncertainties in the solution are calculated through a Monte Carlo simulation, where the data are perturbed by their uncertainties and the inversion is repeated 1000 times.

3.2.1 Datasets and model construction

The block model contains 379 blocks and 923 faults. The block and fault data are subsets of seamlessly interlocking datasets representing different parts of North America and the Pacific, as part of an in–progress global modeling project. Spatially, the block model extends quite far outside of the study region (Figure 5), to fully capture the motion of major plates and to eliminate the possibility of unmodeled elastic locking from outside the model affecting results (i.e., locking on the San Andreas or southern Cascadia affecting estimated block motions and subduction locking patterns in central and northern Cascadia, or the Alaska subduction zone affecting rates on the Fairweather and Denali faults).

The block model uses two types of data, GNSS, which includes Global Positioning System data, and geologic slip rates. Both data types were compiled from a variety of sources, described below, some of which are themselves compilations. Additionally, the motion of the Explorer plate is controlled by the Explorer-North America pole from Braunmiller and Nábělek (2002).

The model uses 427 geologic slip rates. The slip rates are either Quaternary rates from crustal faults (generally from offset Quaternary geologic units) and minor data from the Queen Charlotte Transform and Chatham Strait fault, or 0.78 Ma–present mid–ocean spreading rates derived from seafloor magnetic anomalies on the Juan de Fuca ridge, describing relative motions between the Pacific, Juan de Fuca and Gorda plates (DeMets et al., 2010). With the exception of offshore data, there is one slip rate in Canada (Haeussler et al., 2017), on the Denali fault. Most fault slip rates from the contiguous US are from the compilation by Hatem et al. (2022); others are from Willis et al. (2007); DeMets et al. (2010); Delano et al. (2017); Haeussler et al. (2017); Brothers et al. (2018, 2020); Duckworth et al. (2021); Witter et al. (2021).

The model uses 6911 GNSS velocities. These come from several sources: the compilation by Elliott and Freymueller (2020) for the Alaskan/Queen Charlotte region, the worldwide compilation for the Global Strain Rate Model by Kreemer et al. (2014), and the MIDAS data maintained by University of Nevada Reno (Blewitt et al., 2018). All data are in a well-constrained stable North American reference frame. The data are filtered such that the newest data are used for a single site if the site is present in more than one dataset, with the exception of data clearly contaminated by co- and post-seismic effects from large earthquakes such as the Haida Gwaii event; the Global Strain Rate Model and Elliott datasets are filtered to remove these, but the MIDAS dataset is produced algorithmically (Blewitt et al., 2016) and is not.

A notable characteristic of the deformation data is the sparsity of data in western Canada, especially outside of Vancouver Island and the Vancouver Metropolitan Region. Data sparsity is the largest factor reducing confidence in the modeling results, as the slip rates are unlikely to be well constrained in the absence of measured velocities. This would be particularly problematic if a large slip rate were being inferred on a fault surrounded by sparse data availability. Luckily, this is not observed in this model due to low strain rates suggested by GNSS velocities in the poorly-sampled interior of BC and western NWT.

3.2.2 Results

The block model fits the velocities with a root-mean-square error of 5.1 mm/yr. The mean misfit is 1.7 mm/yr, compared to a mean velocity magnitude of 10.2 mm/yr. The largest misfits are above the shallower part of the subduction zones (especially the Alaskan forearc) where there are high spatial gradients in the geodetic velocity field, suggesting that the model is not perfectly capturing shorter-wavelength variations in subduction zone coupling. The residuals through many other regions are relatively low (less than 2 mm/yr) and show no systematic orientation.

The predicted velocities are shown in Figures S4 and S5. The residuals are shown in Figures S6 and S7. Comparisons of the observed vs. predicted geologic slip rates are shown in Figure S8.

The block modeling yields moderate to low slip rates (<2 mm/yr) throughout Canada (Figure 6), except on the Queen Charlotte transform and its northward extension to the Denali fault. The QCF slips at ∼45 mm/yr, lower than the geologic rates of Brothers et al. (2020) but within uncertainty and well aligned with other recent research (Elliott and Freymueller, 2020).

The Mackenzie thrust slips at 1–2.5 mm/yr (Figure 6). The rates are the highest in the south, near where the Nahanni earthquakes occurred (Figure 1). Shortening rates decrease slightly southward along the Rocky Mountain thrust front, with rates of 1.6±0.5 mm/yr through BC to 1.5±0.5 mm/yr in Alberta. The Rocky Mountain Trench has rates around 0.5 mm/yr, with comparable uncertainties (meaning that a zero rate is marginally within the uncertainty).

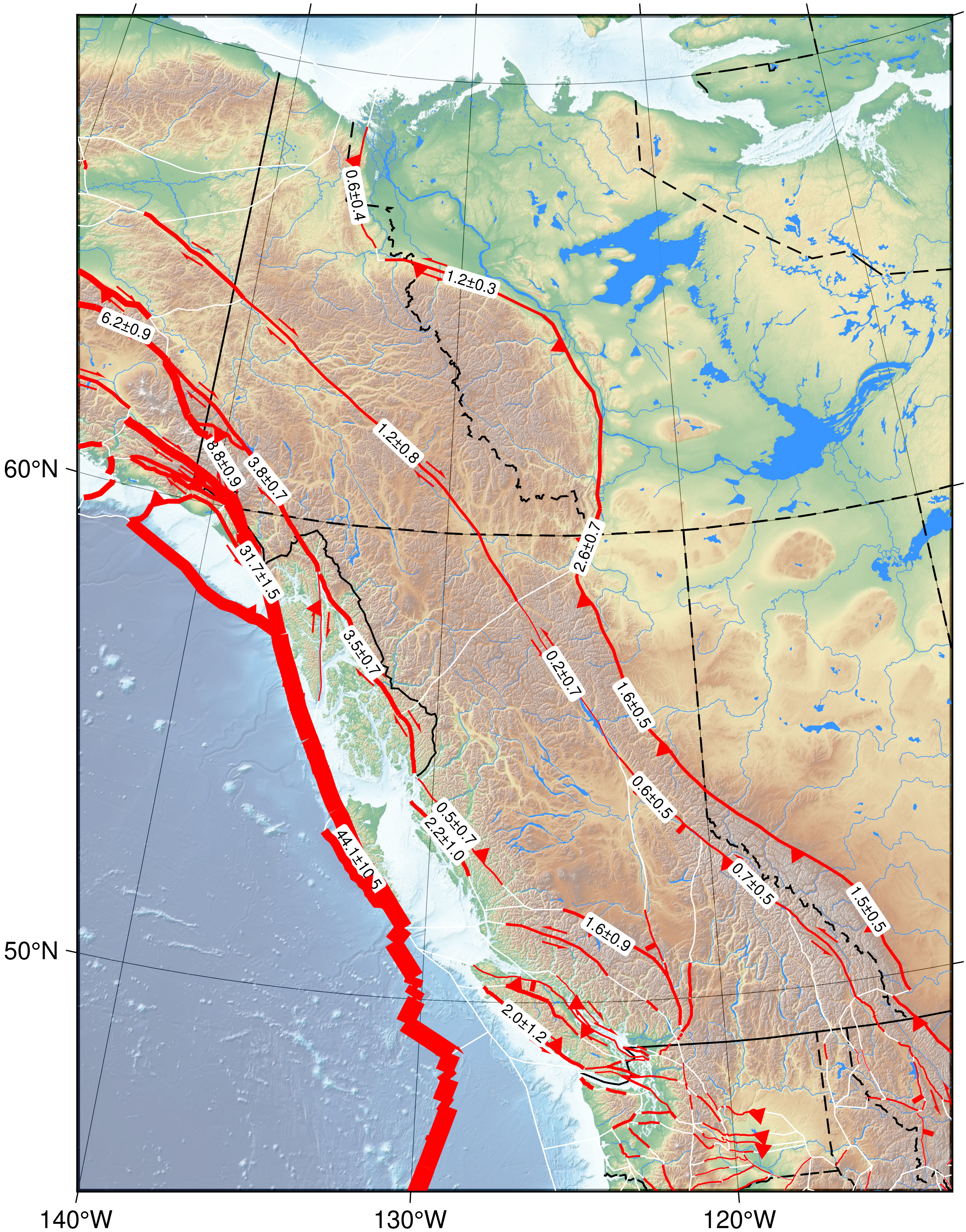

Figure 6 Results from the block modeling inversion. Line thickness on all faults proportional to the square of the slip rate.

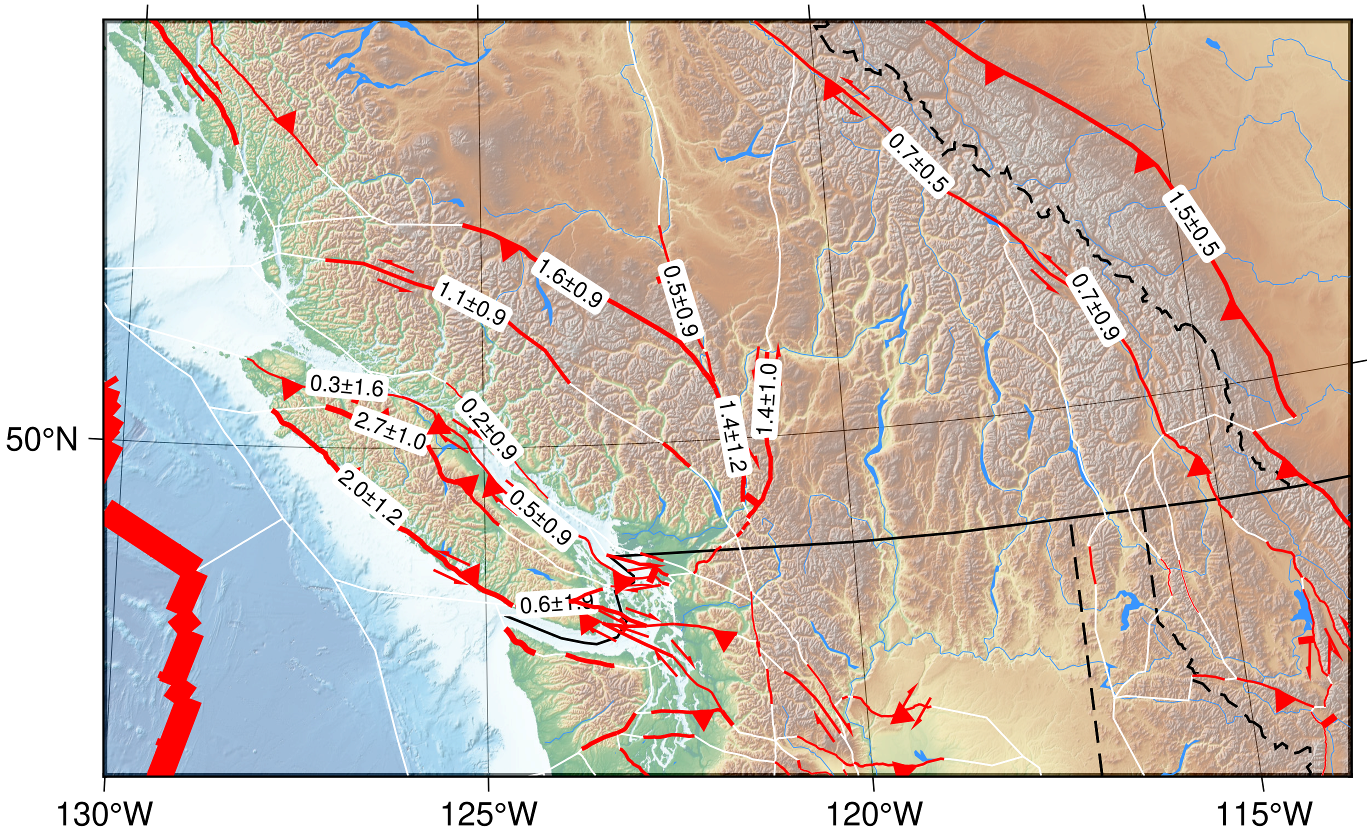

Figure 7 Results from the block modeling inversion. Line thickness on all faults proportional to the square of the slip rate.

Slip rates on the Pacific coast are similar. The Coastal Shear Zone has a 2.2±1.0 rate for the outermost fault, and <0.5 mm/yr for the innermost one (Figure 6, Figure 7). Farther south in the Pacific Ranges, where upper-plate shortening may result from partial locking of northern Cascadia, rates are similar but accommodated on a wider array of faults, and therefore accommodating more net strain across the region (Figure 7).

Slip rates on the longer Vancouver Island faults (the West Coast and Beaufort Range faults) are the highest, 2–2.7 mm/yr. These rates decrease moderately to the south, and dramatically to the east; the San Juan and Leech River faults slip at 0.3–0.6 mm/yr (with large uncertainties), and the Gulf Islands faults are all <1 mm/yr.

The pattern of locking on the Cascadia subduction zone is similar to that seen in other studies (e.g., Graham et al., 2018; Lindsey et al., 2021), with an area of strong locking beneath the Olympic peninsula of WA. Analysis of the locking pattern reveals that the inboard limit of the effects of locking on the geodetic velocities is fairly limited, with rates near zero east of -120°(Figure S9).

3.3 Hazard modeling

3.3.1 Seismic Source Model construction

Our goal in this study is to understand the potential impact of including shallow crustal faults on seismic hazard. These comparisons are best made by adding fault sources derived from the block model to the existing Canada's 6th Generation Seismic Hazard Model (CanSHM6) seismic source model, while modifying the existing seismic source model as minimally as possible; edits are made only to remove duplicated structures and to avoid double counting of seismicity on faults and the area sources they are embedded in.

Because we are not intending to produce a comprehensive, independent PSHA model, we do no formal exploration of the impact of various modeling parameters and strategies, or include them as logic tree branches representing epistemic uncertainty in the seismic source model logic tree. CanSHM6 is used as-is.

The first step in seismic source model construction is to make seismic sources from the block model results. To do this, we use newly-developed tools that are part of the OpenQuake Model Building Toolkit called *Fermi* (Styron et al., 2024). *Fermi* creates fault network models, which allow subfault to multifault ruptures (Field et al., 2015; Chartier et al., 2019), removing strict fault segmentation and its associated issues, such as a restrictive and unrealistic range of earthquake geometries and magnitudes. Fermi works through methods that are similar to previous work, in particular OpenSHA's Fault System Tools, developed as part of UCERF (Field et al., 2015; Milner et al., 2022).

Each three-dimensional fault surface from the block model, without any geometric simplification, is broken into subfaults (fault patches) as close to 10x10 km as possible, while still dividing the fault surface into equally-sized units. There are 154 faults within the seismic source model (a spatial subset of those in the more expansive block model), and these are divided into 3041 subfaults. Each of these subfaults can rupture independently, forming the smallest ruptures in the fault sources. Then, larger ruptures are created by assembling rectangular collections of subfaults on each fault (conforming to rupture aspect ratio limitations). These single-fault ruptures may then also be joined to form multifault ruptures, which are sets of single-fault ruptures that occur together in the PSHA model, as long as each rupture in the set is less than a specified 'jump distance' of 10 km from another rupture. We have imposed a maximum of 7 single-fault ruptures within each multifault rupture. This produces millions of ruptures, so we limit multifault ruptures to those those that only involve full–fault single–fault ruptures. The multifault ruptures are then assigned plausibilities based on how well connected the linked faults are in terms of jump distance, rupture geometry, and slip–azimuth consistency.

Then, the rupture set is filtered to remove the few ruptures with magnitudes below M_w 6.0, as these are modeled by the area sources. This yields 38,785 unique ruptures.

The long-term occurrence rate for every rupture is found by solving for rates that sum to the seismic slip rate on each subfault (Figure S10), as well as fitting a model–wide magnitude–frequency distribution (Figure S11) moment balanced to the summed seismic slip rates for all faults. The seismic slip rate is the fraction of the total slip rate on the fault that represents slip released in mainshocks, discounting the fraction released through aftershocks, afterslip, interseismic creep, and other processes which are less seismically hazardous; we have used 0.7 as the seismic fraction, which is a value that in our experience works well in many orogens worldwide that have more well–studied fault networks as well as more frequent and therefore better characterized seismicity.

3.3.2 Merging of faults and area sources

Once the fault sources have been created and the rupture rates found through inversion, the new fault sources and existing seismic source model must be merged. The existing model comprises both distributed (area) sources and fault (planar) sources. Every fault source in the existing CanSHM6 model is represented in the block model. To maximize internal consistency, we replace all faults in the model, with the exception of those representing the Cascadia and Alaska-Aleutian subduction systems (as differences in the modeling strategies for subduction may mask the effects of including crustal faults in key areas of the model).

The rest of the original CanSHM6 seismic source model is composed of area sources. Block model faults that do not directly replace existing faults are within one or more area sources, and in principle, model the same earthquakes. Therefore, we must avoid ‘double counting’ seismicity, i.e. having multiple sources in the model capable of producing the same seismicity. The area sources in the model are calibrated on the instrumental seismic catalog, and therefore produce all of the seismicity within their borders. Small to moderate magnitude seismicity is found throughout the area sources, but larger earthquakes are typically within about 20 km distance of mapped faults. Therefore, we have reduced the rates of ruptures above M_w 6.0 by 80% in area sources with modeled faults inside, generally consistent with the accepted premise that large earthquakes will generally occur on faults (e.g. Adams and Clague, 1993). This allows for some higher-magnitude seismicity to occur throughout the modeled region, but the majority of this seismicity will occur on the faults with rates derived from the deformation modeling results. Area sources without substantial faulting in their interiors are unchanged.

It should be noted that this approach does not involve balancing total moment release rate to ensure it is preserved between the stock and block models. This is not considered because the seismic catalog used for CanSHM6 is only about 150 years: not sufficiently long to include moment released from large crustal earthquakes on all fault sources (Halchuk et al., 2015a).

The CanSHM6 seismic source model logic tree contains 6 branches, corresponding to epistemic uncertainties in the characterization of seismicity in eastern Canada. The sources for eastern Canada do not contribute to hazard in or near western Canada, so we have removed those sources from the source model and ground motion logic trees. Only one source model branch is present for the west; we have modified this.

The CanSHM6 also uses a ground motion model that requires a slightly customized version of the OpenQuake Engine. However, small modifications to the ground motion model have been made that allow it to be used (and included) with the standard version of the OpenQuake Engine (Pagani et al., 2014), while producing virtually identical results for western Canada. We have used this modified GMM with the OpenQuake Engine (version 3.24.0-git29b7ce8d46) for all hazard and risk calculations.

3.3.3 Hazard results

The hazard map showing the peak ground acceleration (PGA) measured in g at a 10% exceedance rate in 50 years from the block model is shown in Figure 8. The map showing the same metric from the stock CanSHM6 model is shown in Figure 9. Figure 10 shows the change in PGA from the stock to the block model.

The first-order result is that the hazard map produced by the block model is quite similar to that produced by the stock model. This indicates that the inclusion of the faults does not dramatically change the expectations of ground shaking in western Canada.

However, there are some second-order changes. Hazard has increased near the fault traces throughout much of the study area, which is not surprising. The increase is largest in southern BC, particularly in the interior of Vancouver Island, due to the Beaufort Range fault (Lynch et al., 2025), the southeastern Pacific Ranges and the adjacent Thompson Plateau, and the southernmost Rocky Mountain Trench.

There is also a hazard increase along the Coastal Shear Zone in Alaska, and the central and parts of the Mackenzie thrust front, where slip rates are relatively high as well. The block modeling results indicate a transfer of strain from the central Denali fault down through the Fairweather and northern QCF, leading to an increase in hazard on those

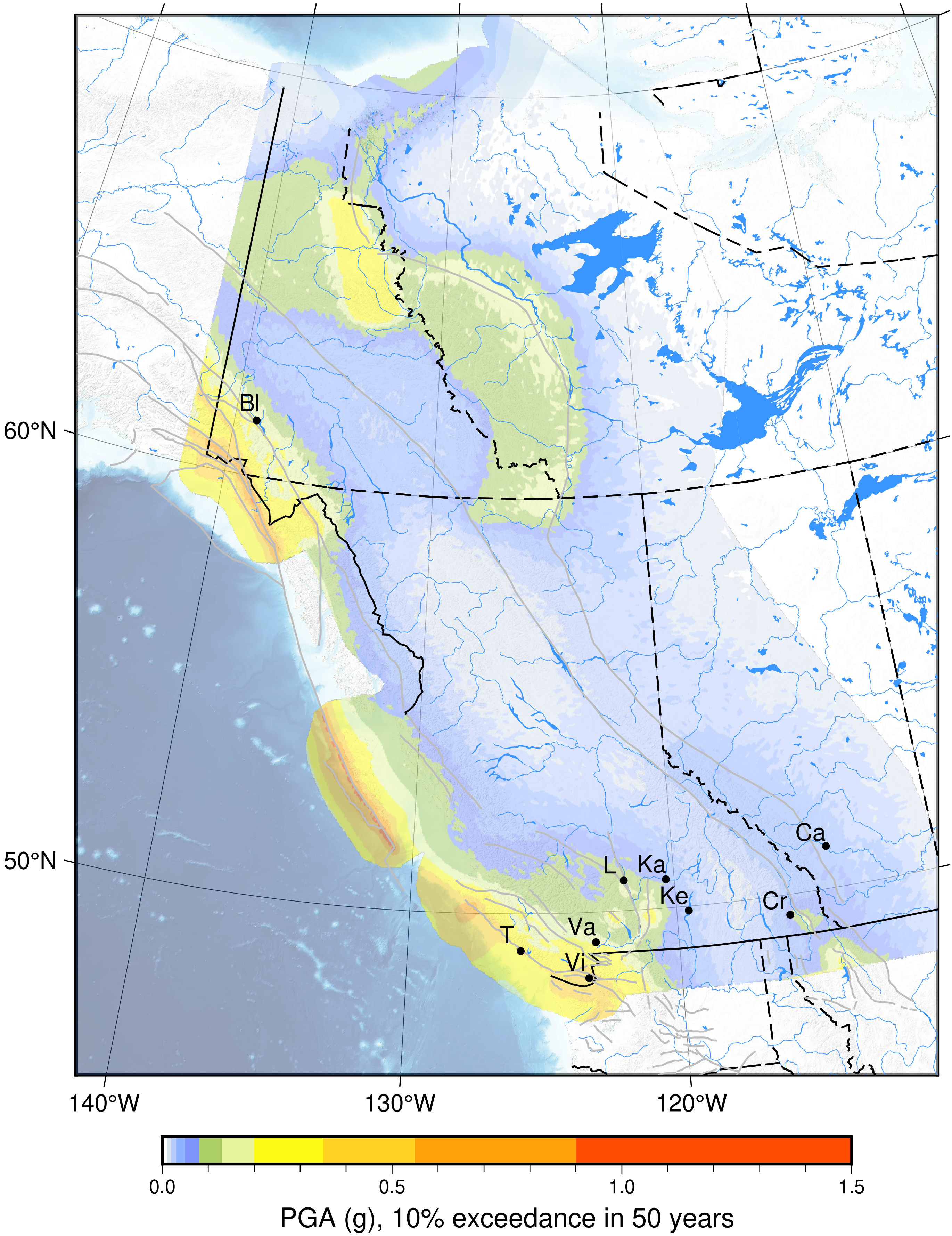

Figure 8 Peak Ground Acceleration (g) for an exceedance rate of 10% in 50 years, from the Canada block model.

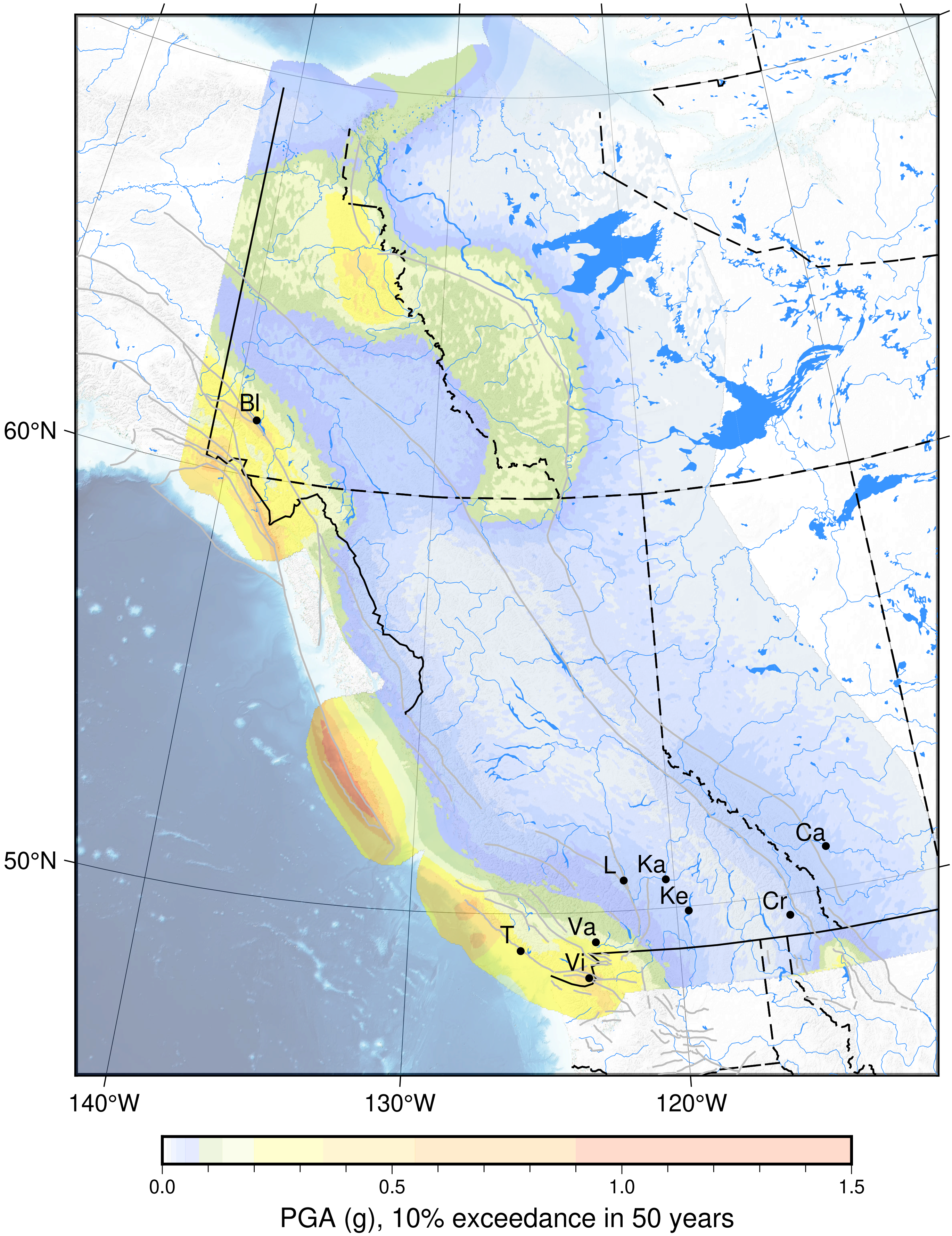

Figure 9 Peak Ground Acceleration (g) for an exceedance rate of 10% in 50 years, from the stock Canada model (SHM6).

faults and a decrease in hazard on the eastern Denali fault in the Yukon Territory (though in absolute terms, the hazard is still quite high).

The largest change, in absolute terms, is a decrease in the hazard just west (offshore) of Haida Gwaii, and a substantial increase to the south of the archipelago. The decrease in hazard in Haida Gwaii seems to be related to CanSHM using a higher activity for the Haida Gwaii Thrust than what is observed in geologic constraints, which provide the primary control on the block model inversion there.

At the 2% exceedance probability in 50 years, which is relevant to Canada's building codes, the patterns of change are similar (Figures S12, S13, S14). The discrepancies are larger, because faults become more of a determinant of hazard at higher return periods.

We have selected nine communities for more in-depth analysis, indicated in Figures 8, 9, and 10. These communities were chosen either to highlight the differences in hazard between the models, or because they represent a substantial fraction of the population in the study area. Due to the data sparsity and other uncertainties in the fault modeling, described above, we view these results as illustrative rather than prescriptive: they demonstrate the potential for changes to seismic hazard in western communities, which may motivate continued study of potentially active faults. Hazard curves for PGA were calculated at these cities for the stock CanSHM6 model, the block model (Figure 11).

The hazard curves in Figure 11 show that for many of the study sites, especially those with relatively high hazard in the stock model, the change in hazard is minor. In particular, for Vancouver (the largest population center in the study area), the hazard curves are almost identical. The other communities in the Cascadia region (Victoria and Tofino) are similar, because their hazard is largely influenced by the Cascadia subduction zone rather than much smaller and slower-moving crustal faults. The other high–hazard site, Burwash Landing (on the eastern Denali fault), saw a decrease in hazard as the block model transfers central Denali strain south along the Fairweather Fault rather than along the Denali Fault system to the southeast.

The communities in the interior of southern BC and Alberta saw mild to strong increases in hazard in the fault model, with the magnitude of increase influenced by their distance to major faults, and the rupture behavior of those faults. Of the ten cities considered, Kelowna and Calgary showed the smallest increases, though the hazard curve at Calgary (as well as Lillooet) shows a much more dramatic increase at higher return periods, indicating the influence of relatively strong but infrequent earthquakes. This is also seen at Tofino, where the Cascadia megathrust shows a similar influence on hazard. The changes at Kamloops and Cranbrook are larger at moderate return periods, due to more frequent but smaller–magnitude seismicity on nearby faults.

3.4 Risk Modeling

To better understand the implications of the change in hazard, a probabilistic risk assessment was undertaken for several key cities in western Canada. The assessment is based on Canada's National Seismic Risk Model (Hobbs et al., 2023), using the stochastic risk calculator of the OpenQuake Engine (Pagani et al., 2014) to evaluate the financial losses at return periods of 475, 2475, and 4975 years — equivalent to a 10%, 2%, and 1% probability of exceedance in 50 years, respectively. The site conditions (Allen and Wald, 2009), vulnerability functions (Hobbs et al., 2023) and exposure model (Journeay et al., 2022) are identical to those in the National Risk Model. The hazard model for risk calculations

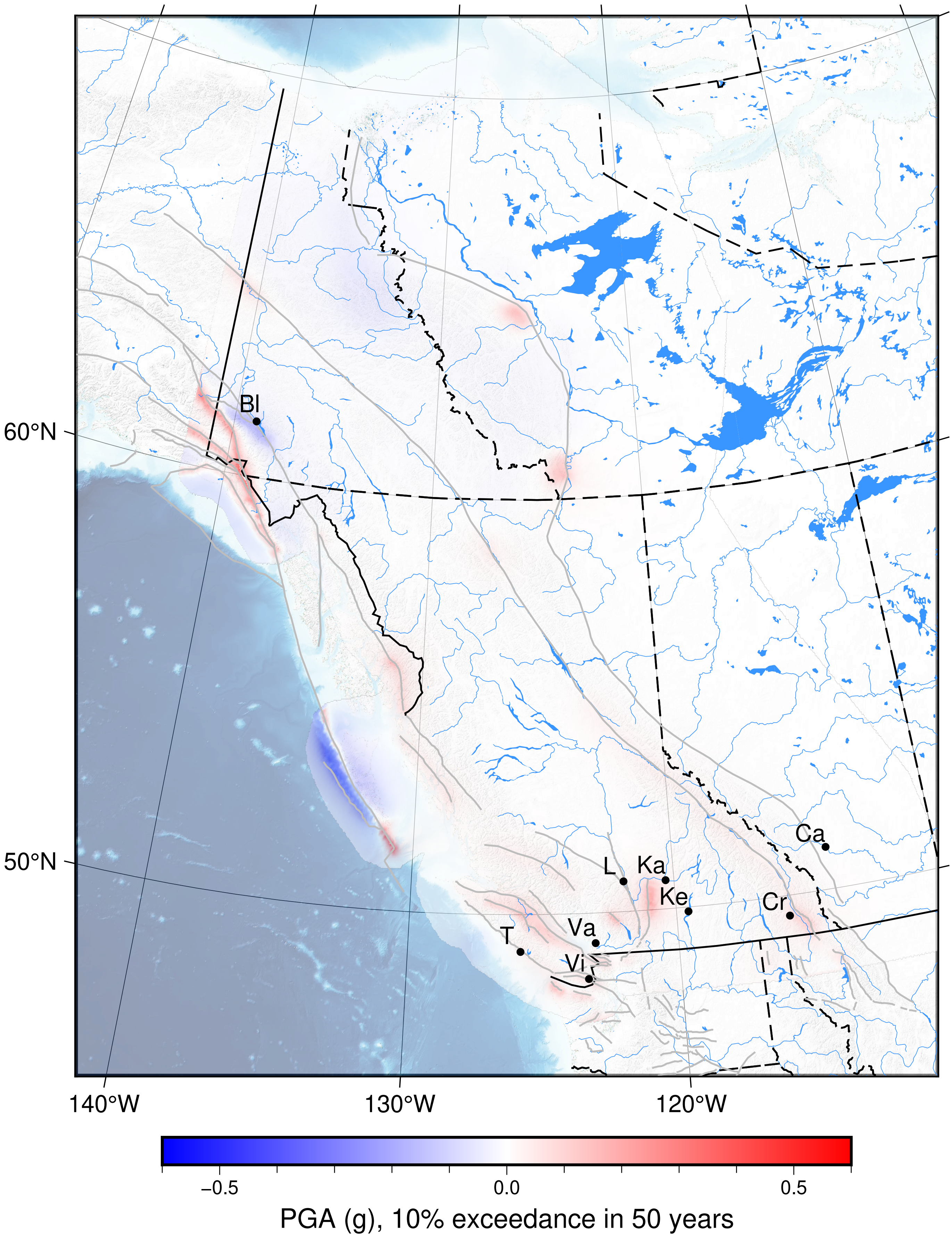

Figure 10 Difference in PGA (g) from the stock model (Figure 9) minus the block model (Figure 8). Positive values (red) indicate an increase in hazard from the block model compared to the stock model, while positive values (blue) indicate a decrease in hazard from the block model compared to the stock model.

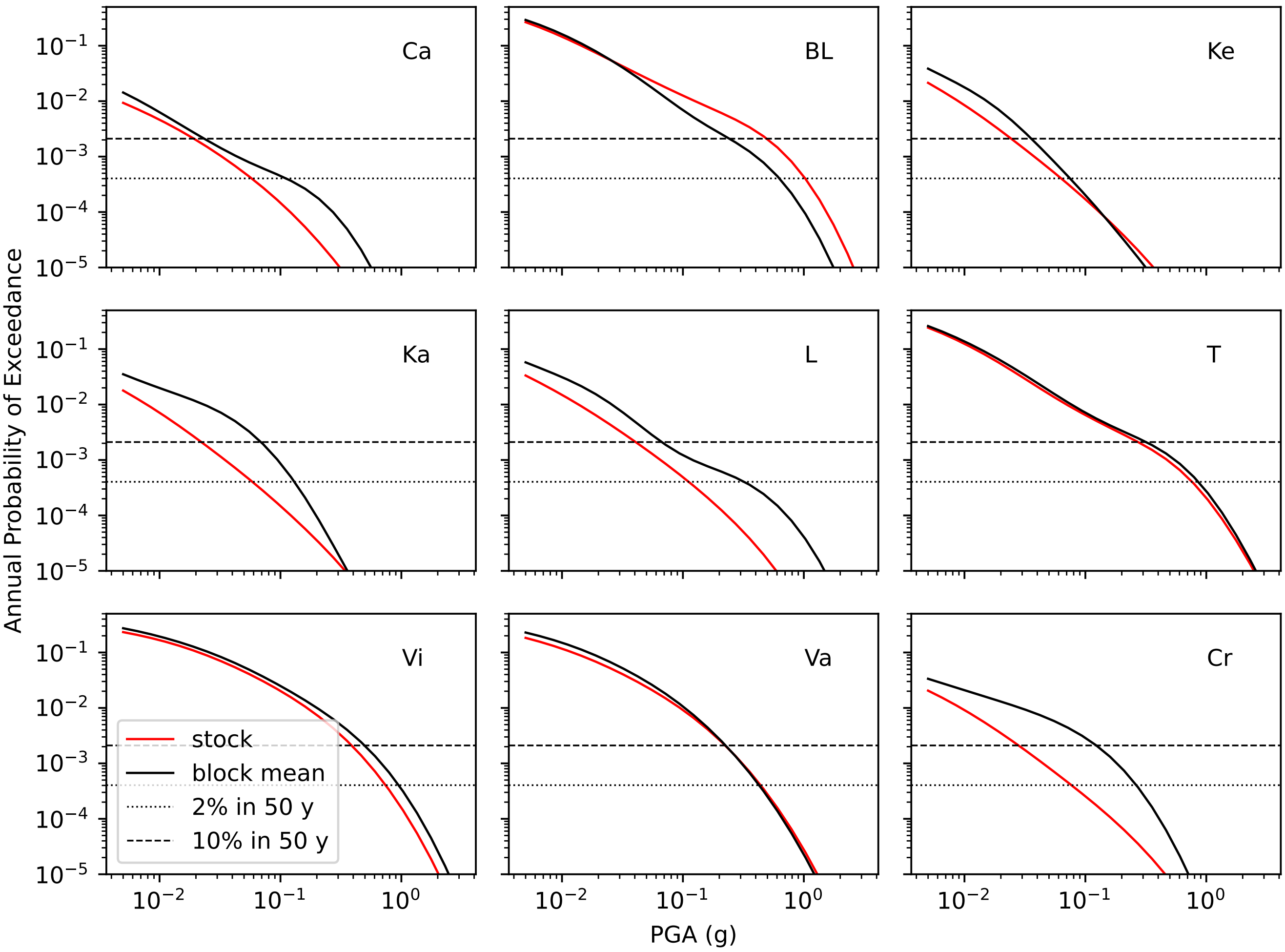

Figure 11 Hazard curves for selected communities. The mean block model is in black. The stock model is in red. Ca=Calgary. BL=Burwash Landing. Ke=Kelowna. Ka=Kamloops. L=Lillooet. T=Tofino. Vi=Victoria. Va=Vancouver. Cr=Cranbrook.

is abridged to include only the western portion (Kolaj et al., 2023), as was done for the hazard calculations. This allows for greater proportional sampling of the western logic tree without wasted computations, without affecting the results within the area of interest for this study. Specifically, this is achieved by limiting the hazard model to only one of the six logic tree branches, given that the western model is the same in all six, and then removing stable crustal fault sources from the source model file. This is done for the “stock" and “block" versions of the model.

Risk is assessed, alphabetically, in Calgary, Alberta; Cranbrook, BC; Burwash Landing, Yukon; Lillooet, BC; Kamloops, BC; Kelowna, BC; Tofino, BC; Vancouver, BC; and Victoria, BC. These are locations (Table 1) that demonstrate the impact of the change in hazard between the existing 2020 National Building Code of Canada (NBCC2020) model and the block model described herein. Some of them are major cities with population over 100,000 (e.g. Calgary, Vancouver, and Kelowna) with the potential for large impacts on the provincial or national economy, whereas others are small cities or towns located nearby to faults considered in this model. There is also a large difference between the climates experienced by these locations, with some having almost Mediterranean conditions and others facing prolonged near-arctic winters. Climate information is also provided in Table 1, as the impact of an earthquake has the potential to be significantly more serious if harsh conditions do not permit sheltering in place without power or camping outdoors, such as would be the case during winter most of the cities considered.

	Pop.	Asset Value	# Bldgs.	Coldest Temp.	Hottest Temp.
Burwash Landing	100	30	45	-44.7	26.0
Tofino	1900	821	671	-5.7	25.8
Victoria	86900	38777	14471	-6.4	30.2
Vancouver	631700	197695	93999	-9.3	29.7
Lillooet	2300	1019	1077	-24.6	31.3
Kamloops	90300	27937	27182	-24.4	35.8
Kelowna	127400	44534	34851	-19.7	35.6
Cranbrook	20100	8300	7500	-27.0	33.1
Calgary	1239700	263174	325529	-33.6	31.9

Table 1 Exposure of select cities considered. Population (‘Pop.’, nighttime) to nearest hundred, Asset Value (in millions 2019 CAD), and Number of Buildings (‘# Bldgs.’) are taken from the exposure model used herein (Journeay et al., 2022). Temperatures (‘Temp.’) are the hottest and coldest daily temperatures observed in a 30 year period from 1981-2010, from www.climatedata.ca, reported in degrees Celsius.

3.4.1 Risk Modeling Results

The results of the risk analysis for select cities are shown in terms of loss exceedance curves in Figure 12 and Table 2. While the “block" model strongly increases the risk for some locations (e.g. Calgary, Cranbrook, and Lillooet, where the “block” loss and its uncertainty is outside of the uncertainty of the “stock" model), it has a muted impact at other locations (e.g. Vancouver, Victoria, Tofino, and Kelowna) and actually decreases the risk slightly at Burwash Landing in the Yukon.

These results highlight that there is a potential for a sizeable increase in risk across western Canada from incorporating geodetic data into hazard models, particularly in the interior of BC and east through the Rocky Mountains. Given that BC has the highest risk of any province in Canada, this increase could exacerbate the known issue that the expected 500–year loss across the country is will potentially exceed the capacity of the property and casualty insurance sector to remain solvent (Hobbs et al., 2023; Kelly et al., 2013). As shown in Table 2, mean 475 year losses in Calgary and Lillooet would be 1.3 and 2.3 times larger, respectively, in the block model than in NBCC2020. This certainly underscores the need to better understand the seismic potential of the Rocky Mountain Thrust Front, which

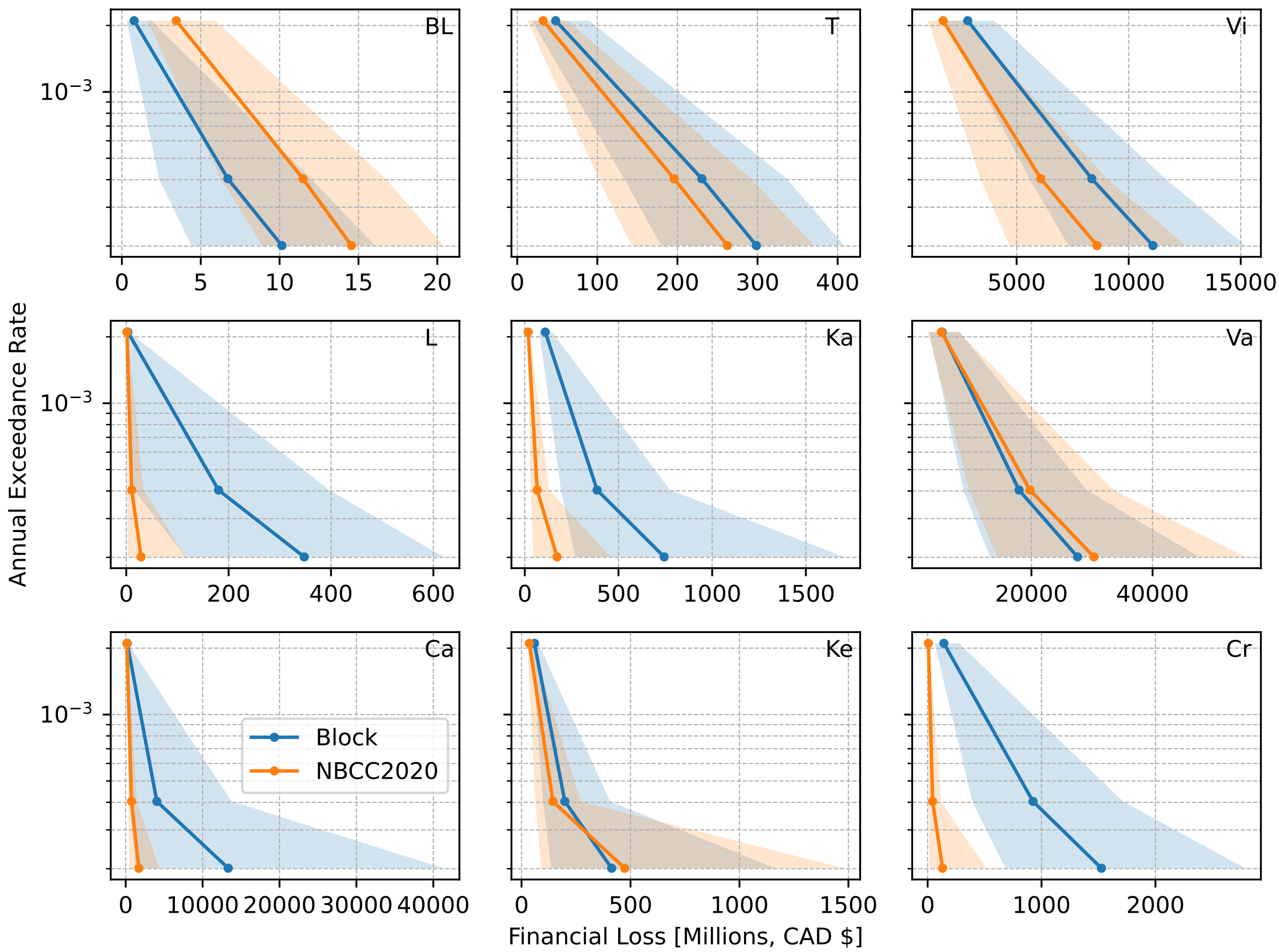

Figure 12 Mean loss exceedances curve for the communities considered in this study, including 5th and 95th percentiles shown by transparency. The “stock" NBCC2020 model is indicated in orange whereas the “block" model described in this study is shown in blue. Ca=Calgary. BL=Burwash Landing. Ke=Kelowna. Ka=Kamloops. L=Lillooet. T=Tofino. Vi=Victoria. Va=Vancouver. Cr=Cranbrook.

runs very close to Calgary. In Cranbrook this increase is estimated to be 20 times larger, given the low level of seismic risk for Cranbrook with the current hazard model. It therefore benefits not only the scientific and engineering communities to better constrain fault slip rates and geodetic locking across western Canada, but also the insurance and finance sectors that hold much of the economic exposure.

	NBCC2020 Model				Block Model			
	AAL	475	2475	4975	AAL	475	2475	4975
Burwash Landing	28	3,453	11,477	14,555	14	776	6,719	10,148
Tofino	334	32,372	195,788	262,309	414	48,024	230,490	298,583
Victoria	18,097	1,721,619	6,079,944	8,588,837	26,450	2,817,542	8,353,524	11,081,008
Vancouver	62,397	5,145,661	19,768,577	30,319,160	71,145	5,256,006	17,952,658	27,616,434
Lillooet	34	1,282	10,633	28,865	205	3,071	180,239	347,674
Kamloops	517	18,245	66,231	172,161	1,510	109,225	386,041	744,159
Kelowna	1,071	35,839	143,927	473,416	1,692	59,166	198,508	413,567
Cranbrook	169	7,116	43,668	131,238	1,537	142,896	925,049	1,525,965
Calgary	2,745	149,234	755,484	1,709,729	8,356	201,784	4,048,147	13,333,218

Table 2 Mean risk modeling results, in thousands 2019 CAD, by municipality, for Average Annual Loss (AAL), and return period losses of 475, 2475, and 4975 years. All values are rounded to nearest thousand.

4 Discussion and conclusions

4.1 Discussion

The research presented in this paper constitutes our best effort to characterize active and potentially active (or capable) faulting throughout the entirety of western Canada given the available data, and then assess the impact of those faults on seismic hazard and risk in the region, as represented by the changes to CanSHM6 and Canada's 1st Generation Seismic Risk Model (CanSRM1). Due to data sparsity throughout much of the study area, there is a great deal of remaining epistemic uncertainty in the hazard and risk estimates presented herein. We therefore caution that these findings are best interpreted in a relative sense, to highlight the potential impact of active faulting, rather than a precise assessment of the true hazard or risk. The results suggest that many faults in mainland Canada may be active at rates up to a few mm/yr, consistent with the coherent regional strain field. This is enough to affect seismic hazard near these faults. In areas where faults were already present in CanSHM, the geodetic characterization of these faults produced little effect. For areas closer to the newly–characterized faults, the hazard generally is increased. The pattern of changes in the risk is similar.

The modeled increases in hazard are generally mild to moderate, in an absolute sense. Given the estimated activity level of the faults, much of the study region would be elevated from a fairly low to a moderate seismic hazard region, such that it more closely resembles Washington to the south. Nonetheless, the relative changes in hazard and risk at the study communities away from the Cascadia zone range from 1.5 to 20 times the CanSHM levels.

The modeled impacts of geodetically– and geologically–suggested slip along these potentially active faults are, therefore, alarming. However, more work is needed. It must be stated with emphasis that these faults can only be considered potentially active as no criteria was applied to limit the block model to faults with documented Holocene activity. Additionally, the geodetic network outside of the Cascadia region is extremely sparse. The slip rates on many of the faults are determined by a small number of GNSS stations which are located primarily for accessibility rather than for optimal determination of active deformation patterns and rates. This is quite understandable given the terrain; however, similarly large and challenging tectonic provinces such as Tibet have had more comprehensive geodetic monitoring for decades (e.g., Zhang et al., 2004; Gan et al., 2007). Though paleoseismological investigations of some faults are purported to exist in the grey literature, such as engineering reports, relatively little peer-reviewed, publicly available, research is available to confirm or conclusively deny Quaternary fault activity, much less provide slip rates or recurrence intervals on many of the faults considered herein.

We strongly suspect that further investigation of these faults will substantially modify the results presented here. It is our hope that this study will motivate such work. For example, we think it possible that with additional data, the apparent strain throughout eastern BC into western AB, manifested here as slip on the Rocky Mountain Trench and thrust front, may be reduced. However, since it has been a persistently observed signal for years (e.g., Mazzotti et al., 2011), it clearly warrants dedicated and urgent attention.

Canada is a developed nation with a strong history of seismic hazard assessment to improve public safety. The increases in expected losses caused by the consideration of these potentially active faults (Table 2) are many orders of magnitude larger than the costs associated with more study. Obviously, simply studying the faults will not directly reduce losses, but no amelioration of the risk will occur in the absence of the information necessary to firmly quantify the hazard, particularly in regions which are currently believed to be low risk. Increasing both the density of the geodetic coverage over the Cordillera, through continuous and campaign GNSS stations, and targeted paleoseismic or neotectonic investigations on specific faults would be useful and complementary.

4.2 Conclusions

We have synthesized the available geologic and geodetic data on active and potentially active faults throughout western Canada through the use of a block model to characterize the fault slip rates. Subsequently, we modified the existing Canadian seismic hazard model (CanSHM) to include these faults, and calculated seismic hazard and risk consistently with both the 'stock' and 'block' models in order to assess the impacts of the potentially active faults on the hazard and risk.

Results are summarized with the following points:

1. The geodetic data and block model suggest low to moderate slip rates (up to a few mm/yr) on potentially active faults across western Canada.

2. Increases in seismic hazard and risk due to consideration of potentially active faults are low to moderate in absolute terms, but away from the Cascadia subduction zone, the increases are much larger in relative terms. This is particularly noticeable in communities near newly modeled faults, such as Lillooet and Calgary.

3. The sparsity of data used to constrain the solutions greatly limits confidence in the results. Given the scale of the increases to hazard, renewed data collection efforts should be undertaken to reduce uncertainty and enable the management of potential hazards in the region.

Acknowledgements

We thank Michal Kolaj for comments on a draft version of this work. Some figures were made with PyGMT (Uieda et al., 2021) and GMT (Wessel et al., 2019).

Author Contributions

RS, TH, and MJ all conceived of the study. RS mapped the faults and blocks in consultation with MJ and TH. RS performed the block and hazard modeling. TH performed the risk modeling. RS and TH wrote the manuscript.

Data and code availability

The data and script for the block model can be found at https://github.com/cossatot/cascadia_blocks, and need the Oiler code to run, which is at https://github.com/cossatot/Oiler. The source files for the stock hazard model (CanSHM) are not publicly available but are described by Kolaj et al. (2020). The block hazard model, risk model, stock and block hazard and risk results, and associated scripts are found at https://github.com/cossatot/cnf-all. These need the OpenQuake Model Building Toolkit (https://github.com/GEMScienceTools/oq-mbtk) and the OpenQuake Engine (https://github.com/gem/oq-engine).

Conflicts of Interest

We declare that there are no conflicts of interest.

References

Adams, J. and Clague, J. J. Neotectonics and large-scale geomorphology of Canada. *Progress in physical geography*, 17(2):248–264, 1993.

Allen, T. I. and Brillon, C. Assessment of ground-motion models for use in the British Columbia North Coast region, Canada. *Bulletin of the Seismological Society of America*, 105(2B):1193–1205, 2015.

Allen, T. I. and Wald, D. J. On the use of high-resolution topographic data as a proxy for seismic site conditions (VS 30). *Bulletin of the Seismological Society of America*, 99(2A):935–943, 2009.

Balfour, N., Cassidy, J., and Dosso, S. Crustal anisotropy in the forearc of the northern Cascadia subduction zone, British Columbia. *Geophysical Journal International*, 188(1):165–176, 2012.

Barrie, J. V. and Greene, H. G. The Devils Mountain fault zone: An active Cascadia upper plate zone of deformation, Pacific Northwest of North America. *Sedimentary geology*, 364:228–241, 2018.

Barrie, J. V., Douglas, K., and Molloy, B. Geological hazards off Cape Lazo, eastern Vancouver Island. Open File 8773, Geological Survey of Canada, 2021. doi: 10.4095/328131.

Basham, P. and Newitt, L. A historical summary of Geological Survey of Canada studies of earthquake seismology and geomagnetism. *Canadian Journal of Earth Sciences*, 30(2):372–390, 1993.

Bent, A., Kolaj, M., Ackerley, N., Adams, J., and Halchuk, S. The 2017 Barrow Strait, Arctic Canada, earthquake sequence and contemporaneous regional seismicity. *Seismological Research Letters*, 89(5):1977–1988, 2018.

Blais-Stevens, A., Clague, J. J., Brahney, J., Lipovsky, P., Haeussler, P. J., and Menounos, B. Evidence for large Holocene earthquakes along the Denali fault in southwest Yukon, Canada. *Environmental & Engineering Geoscience*, 26(2):149–166, 2020.

Blewitt, G., Kreemer, C., Hammond, W. C., and Gazeaux, J. MIDAS robust trend estimator for accurate GPS station velocities without step detection. *Journal of Geophysical Research: Solid Earth*, 121(3):2054–2068, 2016.

Blewitt, G., Hammond, W., and Kreemer, C. Harnessing the GPS data explosion for interdisciplinary science. *Eos*, 99(2):e2020943118, 2018.

Braunmiller, J. and Nábělek, J. Seismotectonics of the Explorer region. *Journal of Geophysical Research: Solid Earth*, 107(B10):ETG–1, 2002.

Brothers, D. S., Elliott, J. L., Conrad, J. E., Haeussler, P. J., and Kluesner, J. W. Strain partitioning in southeastern Alaska: Is the Chatham Strait fault active? *Earth and Planetary Science Letters*, 481:362–371, 2018.

Brothers, D. S., Miller, N. C., Barrie, J. V., Haeussler, P. J., Greene, H. G., Andrews, B. D., Zielke, O., Watt, J., and Dartnell, P. Plate boundary localization, slip-rates and rupture segmentation of the Queen Charlotte Fault based on submarine tectonic geomorphology. *Earth and Planetary Science Letters*, 530:115882, 2020.

Cassidy, J., Rogers, G., Lamontagne, M., Halchuk, S., and Adams, J. Canada's Earthquakes: 'The Good, the Bad, and the Ugly'. *Geoscience Canada*, 37(1):1–16, 2010.

Cassidy, J. F. and Bent, A. L. Source parameters of the 29 May and 5 June, 1940 Richardson Mountains, Yukon Territory, earthquakes. *Bulletin of the Seismological Society of America*, 83(3):636–659, 1993.

Chartier, T., Scotti, O., and Lyon-Caen, H. SHERIFS: Open-source code for computing earthquake rates in fault systems and constructing hazard models. *Seismological Research Letters*, 90(4):1678–1688, 2019.

Chase, C. The N plate problem of plate tectonics. *Geophysical Journal International*, 29(2):117–122, 1972.

Clowes, R., Brandon, M., Green, A., Yorath, C., Brown, A. S., Kanasewich, E., and Spencer, C. LITHOPROBE—southern Vancouver Island: Cenozoic subduction complex imaged by deep seismic reflections. *Canadian Journal of Earth Sciences*, 24(1):31–51, 1987.

Coleman, M. E. and Parrish, R. R. Eocene dextral strike-slip and extensional faulting in the Bridge River terrane, southwest British Columbia. *Tectonics*, 10(6):1222–1238, 1991.

Dash, R., Spence, G., Riedel, M., Hyndman, R., and Brocher, T. Upper-crustal structure beneath the Strait of Georgia, southwest British Columbia. *Geophysical Journal International*, 170(2):800–812, 2007.

Delano, J. E., Amos, C. B., Loveless, J. P., Rittenour, T. M., Sherrod, B. L., and Lynch, E. M. Influence of the megathrust earthquake cycle on upper-plate deformation in the Cascadia forearc of Washington State, USA. *Geology*, 45(11):1051–1054, 2017.

DeMets, C., Gordon, R. G., and Argus, D. F. Geologically current plate motions. *Geophysical journal international*, 181(1):1–80, 2010.

Dokht, R. M., Smith, B., Kao, H., Visser, R., and Hutchinson, J. Reactivation of an intraplate fault by mine-blasting events: Implications to regional seismic hazard in Western Canada. *Journal of Geophysical Research: Solid Earth*, 125(6):e2020JB019933, 2020.

Doser, D. I. Seismicity of southwestern Yukon, Canada, and its relation to slip transfer between the Fairweather and Denali fault systems. *Tectonophysics*, 611:121–129, 2014.

Douglas, K., Barrie, J., Dill, T., Fralic, T., and Koshure, N. 2021004PGC cruise report: mapping Salish Sea marine geohazards, British Columbia. Technical Report Open File 8865, Geological Survey of Canada, 2022. doi: 10.4095/329621.

Drennon, H., Ferrini, V., and Morton, J. J. Multibeam Data Curation and Access Through the Global Multi-Resolution Topography (GMRT) Synthesis. In *OCEANS 2023-MTS/IEEE US Gulf Coast*, pages 1–4. IEEE, 2023.

Drooff, C. and Freymueller, J. T. New insights into the active tectonics of the Northern Canadian Cordillera from an enhanced earthquake catalog. *Journal of Geophysical Research: Solid Earth*, 128(12):e2023JB026793, 2023.

Duckworth, W. C., Amos, C. B., Schermer, E. R., Loveless, J. P., and Rittenour, T. M. Slip and strain accumulation along the Sadie Creek fault, Olympic Peninsula, Washington. *Journal of Geophysical Research: Solid Earth*, 126(3):2020JB020276, 2021.

Ekström, G., Nettles, M., and Dziewoński, A. The global CMT project 2004–2010: Centroid-moment tensors for 13,017 earthquakes. *Physics of the Earth and Planetary Interiors*, 200:1–9, 2012.

Elliott, J. and Freymueller, J. T. A block model of present-day kinematics of Alaska and western Canada. *Journal of Geophysical Research: Solid Earth*, 125(7):e2019JB018378, 2020.

Evans, E. L. A dense block model representing western continental United States deformation for the 2023 update to the National Seismic Hazard Model. *Seismological Society of America*, 93(6):3024–3036, 2022.

Field, E. H., Biasi, G. P., Bird, P., Dawson, T. E., Felzer, K. R., Jackson, D. D., Johnson, K. M., Jordan, T. H., Madden, C., Michael, A. J., et al. Long-term time-dependent probabilities for the third Uniform California Earthquake Rupture Forecast (UCERF3). *Bulletin of the Seismological Society of America*, 105(2A):511–543, 2015.

Finley, T. D., Johnston, S. T., Unsworth, M. J., Banks, J., and Pana, D.-I. Modern dextral strain controls active hydrothermal systems in the southeastern Canadian Cordillera. *Bulletin*, 135(7-8):2015–2037, 2023.

Gan, W., Zhang, P., Shen, Z.-K., Niu, Z., Wang, M., Wan, Y., Zhou, D., and Cheng, J. Present-day crustal motion within the Tibetan Plateau inferred from GPS measurements. *Journal of Geophysical Research: Solid Earth*, 112(B8), 2007.

Gerstenberger, M. C., Marzocchi, W., Allen, T., Pagani, M., Adams, J., Danciu, L., Field, E. H., Fujiwara, H., Luco, N., Ma, K.-F., et al. Probabilistic seismic hazard analysis at regional and national scales: State of the art and future challenges. *Reviews of Geophysics*, 58(2): e2019RG000653, 2020.

Gosselin, J. M., Biegel, K. M., Dettmer, J., Hersh, G., Colpron, M., and Enkelmann, E. Crustal stress near the Yakutat microplate collision from probabilistic earthquake focal mechanisms. *Canadian Journal of Earth Sciences*, (ja), 2024.

Graham, S. E., Loveless, J. P., and Meade, B. J. Global plate motions and earthquake cycle effects. *Geochemistry, Geophysics, Geosystems*, 19(7):2032–2048, 2018.

Greene, H. G., Barrie, J. V., and Todd, B. J. The Skipjack Island fault zone: An active transcurrent structure within the upper plate of the Cascadia subduction complex. *Sedimentary Geology*, 378:61–79, 2018.

Haeussler, P. J., Matmon, A., Schwartz, D. P., and Seitz, G. G. Neotectonics of interior Alaska and the late Quaternary slip rate along the Denali fault system. *Geosphere*, 13(5):1445–1463, 2017.

Halchuk, S., Allen, T., Rogers, G., and Adams, J. Seismic Hazard Earthquake Epicentre File (SHEEF2010)used in the Fifth Generation Seismic Hazard Maps of Canada. *Geological Survey of Canada Open File 7724*, 2015a.

Halchuk, S., Allen, T. I., Rogers, G. C., and Adams, J. Seismic Hazard Earthquake Epicentre File (SHEEF2010) used in the Fifth Generation Seismic Hazard Maps of Canada. Technical Report Open File Report 7724, Geological Survey of Canada, 2015b.

Harrichhausen, N., Morell, K. D., Regalla, C., Bennett, S. E., Leonard, L. J., Lynch, E. M., and Nissen, E. Paleoseismic trenching reveals Late Quaternary kinematics of the Leech River fault: Implications for forearc strain accumulation in northern Cascadia. *Bulletin of the Seismological Society of America*, 111(2):1110–1138, 2021.

Harrichhausen, N., Finley, T., Morell, K. D., Regalla, C., Bennett, S. E., Leonard, L. J., Nissen, E., McLeod, E., Lynch, E. M., Salomon, G., et al. Discovery of an Active Forearc Fault in an Urban Region: Holocene Rupture on the X EOL X ELE K-Elk Lake Fault, Victoria, British Columbia, Canada. *Tectonics*, 42(12):e2023TC008170, 2023.

Hatem, A. E., Collett, C. M., Briggs, R. W., Gold, R. D., Angster, S. J., Field, E. H., and Powers, P. M. Simplifying complex fault data for systems-level analysis: Earthquake geology inputs for US NSHM 2023. *Scientific data*, 9(1):506, 2022.

Hayes, G. P., Moore, G. L., Portner, D. E., Hearne, M., Flamme, H., Furtney, M., and Smoczyk, G. M. Slab2, a comprehensive subduction zone geometry model. *Science*, 362(6410):58–61, 2018.

Hobbs, T. E., Journeay, J. M., Rao, A. S., Kolaj, M., Martins, L., LeSueur, P., Simionato, M., Silva, V., Pagani, M., Johnson, K., et al. A national seismic risk model for Canada: Methodology and scientific basis. *Earthquake Spectra*, 39(3):1410–1434, 2023.

Horner, R., Wetmiller, R., Lamontagne, M., and Plouffe, M. A fault model for the Nahanni earthquakes from aftershock studies. *Bulletin of the Seismological Society of America*, 80(6A):1553–1570, 1990.

Hyndman, R., Cassidy, J., Adams, J., Rogers, G., and Mazzotti, S. Earthquakes and seismic hazard in the Yukon-Beaufort-Mackenzie. *CSEG Recorder*, 30(5):32–66, 2005.

Journeay, J. and Friedman, R. The Coast Belt thrust system: evidence of Late Cretaceous shortening in southwest British Columbia. *Tectonics*, 12(3):756–775, 1993.

Journeay, M., LeSueur, P., and Chow, W. Physical exposure to natural hazards in Canada. 2022.

Kao, H., Shan, S.-J., Bent, A., Woodgold, C., Rogers, G., Cassidy, J. F., and Ristau, J. Regional centroid-moment-tensor analysis for earthquakes in Canada and adjacent regions: An update. *Seismological Research Letters*, 83(3):505–515, 2012.

Kelly, M., Kleffner, A., and Nielson, N. Water, Water Everywhere. *Canadian Underwriter*, 80:12–15, 2013.

Kolaj, M., Adams, J., and Halchuk, S. The 6th generation seismic hazard model of Canada. In *17th world conference on earthquake engineering*, pages 1–12, 2020.

Kolaj, M., Halchuk, S., and Adams, J. Deaggregation of NBCC 2020 Seismic Hazard for Selected Canadian Cities. 2023.

Kreemer, C., Blewitt, G., and Klein, E. C. A geodetic plate motion and Global Strain Rate Model. *Geochemistry, Geophysics, Geosystems*, 15 (10):3849–3889, 2014.

Leonard, L. J., Hyndman, R. D., Mazzotti, S., Nykolaishen, L., Schmidt, M., and Hippchen, S. Current deformation in the northern Canadian Cordillera inferred from GPS measurements. *Journal of Geophysical Research: Solid Earth*, 112(B11), 2007.

Lesage, G., Byrne, K., Morris, W. A., Enkin, R. J., Lee, R. G., Mir, R., and Hart, C. J. Interpreting regional 3D fault networks from integrated geological and geophysical data sets: an example from the Guichon Creek batholith, British Columbia. *Journal of Structural Geology*, 119:93–106, 2019.

Lindsey, E. O., Mallick, R., Hubbard, J. A., Bradley, K. E., Almeida, R. V., Moore, J. D., Bürgmann, R., and Hill, E. M. Slip rate deficit and earthquake potential on shallow megathrusts. *Nature Geoscience*, 14(5):321–326, 2021.

Littel, G. F. and Bostock, M. G. Seismicity at the intersection of the Coast Shear Zone and Anahim Volcanic Belt near Bella Coola, British Columbia, Canada. *Canadian Journal of Earth Sciences*, 60(12):1688–1701, 2023.

Lynch, E., Regalla, C., Morell, K., Harrichhausen, N., and Leonard, L. Evidence for an active transtensional Beaufort Range fault in the northern Cascadia forearc. *Seismica*, 2(4), Aug. 2025. doi: 10.26443/seismica.v2i4.1163.

Lynch, E. M. *Strain Accommodation on Forearc Faults: A Case Study on the Beaufort Range Fault, an Active Crustal Fault in the Northern Cascadia Forearc, Vancouver Island, BC, Canada*. Phd thesis, Northern Arizona University, 2023. Available from ProQuest Dissertations & Theses database. URL: https://www.proquest.com/openview/6d0e412cd3bb22dd1a5aa6e2c55fb046/1?pq-origsite=gscholar&cbl=18750&diss=y.

Mazzotti, S. and Hyndman, R. D. Yakutat collision and strain transfer across the northern Canadian Cordillera. *Geology*, 30(6):495–498, 2002.

Mazzotti, S., Dragert, H., Henton, J., Schmidt, M., Hyndman, R., James, T., Lu, Y., and Craymer, M. Current tectonics of northern Cascadia from a decade of GPS measurements. *Journal of Geophysical Research: Solid Earth*, 108(B12), 2003.

Mazzotti, S., Leonard, L., Cassidy, J., Rogers, G., and Halchuk, S. Seismic hazard in western Canada from GPS strain rates versus earthquake catalog. *Journal of Geophysical Research: Solid Earth*, 116(B12), 2011.

McCaffrey, R., King, R. W., Payne, S. J., and Lancaster, M. Active tectonics of northwestern US inferred from GPS-derived surface velocities. *Journal of Geophysical Research: Solid Earth*, 118(2):709–723, 2013.

McKenzie, D. P. and Parker, R. L. The North Pacific: an example of tectonics on a sphere. *Nature*, 216(5122):1276–1280, 1967.

Meade, B. J. and Hager, B. H. Block models of crustal motion in southern California constrained by GPS measurements. *Journal of Geophysical Research: Solid Earth*, 110(B3), 2005.

Meade, B. J. and Loveless, J. P. Block modeling with connected fault-network geometries and a linear elastic coupling estimator in spherical coordinates. *Bulletin of the Seismological Society of America*, 99(6):3124–3139, 2009.

Merrill, R. J., Bostock, M. G., Peacock, S. M., Schaeffer, A. J., and Roecker, S. W. Complex structure in the Nootka Fault zone revealed by double-difference tomography and a new earthquake catalog. *Geochemistry, Geophysics, Geosystems*, 23(2):e2021GC010205, 2022.

Milne, W. The Snipe Lake, Alberta earthquake of March 8, 1970. *Canadian Journal of Earth Sciences*, 7(6):1564–1567, 1970.

Milner, K. R., Shaw, B. E., and Field, E. H. Enumerating plausible multifault ruptures in complex fault systems with physical constraints. *Bulletin of the Seismological Society of America*, 112(4):1806–1824, 2022.

Monger, J. and Price, R. The Canadian Cordillera: geology and tectonic evolution. *CSEG Recorder*, 27(2):17–36, 2002.

Morell, K., Regalla, C., Amos, C., Bennett, S., Leonard, L., Graham, A., Reedy, T., Levson, V., and Telka, A. Holocene surface rupture history of an active forearc fault redefines seismic hazard in southwestern British Columbia, Canada. *Geophysical Research Letters*, 45(21):11–605, 2018.

Muller, J. E., Cameron, B. E. B., and Northcote, K. E. Geology and Mineral Deposits of the Nootka Sound Map Area (92E), Vancouver Island, British Columbia. Geological Survey of Canada Paper 80-16, Geological Survey of Canada, 1981. doi: 10.4095/119070.

Pagani, M., Monelli, D., Weatherill, G., Danciu, L., Crowley, H., Silva, V., Henshaw, P., Butler, L., Nastasi, M., Panzeri, L., et al. OpenQuake engine: An open hazard (and risk) software for the global earthquake model. *Seismological Research Letters*, 85(3):692–702, 2014.

Personius, S. F., Briggs, R. W., Nelson, A. R., Schermer, E. R., Maharrey, J. Z., Sherrod, B. L., Spaulding, S. A., and Bradley, L.-A. Holocene earthquakes and right-lateral slip on the left-lateral Darrington–Devils Mountain fault zone, northern Puget Sound, Washington. *Geosphere*, 10(6):1482–1500, 2014.

Porter, C., Morin, P., Howat, I., Noh, M.-J., Bates, B., Peterman, K., Keesey, S., Schlenk, M., Gardiner, J., Tomko, K., et al. ArcticDEM. *Harvard dataverse*, 1:2018–30, 2018.

Ramachandran, K. Constraining fault interpretation through tomographic velocity gradients: application to northern Cascadia. *Solid Earth*, 3(1):53–61, 2012.

Ramachandran, K., Dosso, S., Zelt, C., Spence, G., Hyndman, R., and Brocher, T. Upper crustal structure of southwestern British Columbia from the 1998 seismic hazards investigation in Puget Sound. *Journal of Geophysical Research: Solid Earth*, 109(B9), 2004.

Ristau, J., Rogers, G. C., and Cassidy, J. F. Stress in western Canada from regional moment tensor analysis. *Canadian Journal of Earth Sciences*, 44(2):127–148, 2007.

Rogers, G. C. and Ellis, R. M. The eastern British Columbia earthquake of February 4, 1918. *Canadian Journal of Earth Sciences*, 16(7):1484–1493, 1979.

Rogers, G. C. and Hasegawa, H. S. A second look at the British Columbia earthquake of June 23, 1946. *Bulletin of the Seismological Society of America*, 68(3):653–676, 1978.

Snyder, D. B., Roberts, B. J., and Gordey, S. P. Contrasting seismic characteristics of three major faults in northwestern Canada. *Canadian Journal of Earth Sciences*, 42(6):1223–1237, 2005.

Struik, L. Crustal evolution of the eastern Canadian Cordillera. *Tectonics*, 7(4):727–747, 1988.

Styron, R. Contemporary Slip Rates of All Active Faults in the Indo-Asian Collision Zone. *Authorea Preprints*, 2022a.

Styron, R., Pagani, M., Johnson, K., and Bayliss, K. Developing a data-centric workflow for seismic source model construction. In *Seismo-*

logical Research Letters, volume 95, 4 2024. Abstract.

Styron, R. H. Oiler, Oct. 2022b. doi: 10.5281/zenodo.7262453.

Uieda, L., Tian, D., Leong, W. J., Jones, M., Schlitzer, W., Toney, L., Grund, M., Yao, J., Magen, Y., Materna, K., et al. PyGMT: A Python interface for the generic mapping tools. *Zenodo*, 2021.

Umhoefer, P. J. and Schiarizza, P. Latest Cretaceous to early Tertiary dextral strike-slip faulting on the southeastern Yalakom fault system, southeastern Coast Belt, British Columbia. *Geological Society of America Bulletin*, 108(7):768–785, 1996.

Van Zyl, J. J. The Shuttle Radar Topography Mission (SRTM): a breakthrough in remote sensing of topography. *Acta astronautica*, 48(5-12): 559–565, 2001.

Wessel, P., Luis, J. F., Uieda, L. a., Scharroo, R., Wobbe, F., Smith, W. H., and Tian, D. The generic mapping tools version 6. *Geochemistry, Geophysics, Geosystems*, 20(11):5556–5564, 2019.

Willis, J. B., Haeussler, P. J., Bruhn, R. L., and Willis, G. C. Holocene slip rate for the western segment of the Castle Mountain fault, Alaska. *Bulletin of the Seismological Society of America*, 97(3):1019–1024, 2007.

Witter, R. C., Bender, A. M., Scharer, K. M., DuRoss, C. B., Haeussler, P. J., and Lease, R. O. Geomorphic expression and slip rate of the Fairweather fault, southeast Alaska, and evidence for predecessors of the 1958 rupture. *Geosphere*, 17(3):711–738, 2021.

Zhang, P.-Z., Shen, Z., Wang, M., Gan, W., Burgmann, R., Molnar, P., Wang, Q., Niu, Z., Sun, J., Wu, J., et al. Continuous deformation of the Tibetan Plateau from global positioning system data. *Geology*, 32(9):809–812, 2004.